Cell Stem Cell

Short Article

CRISPR-Mediated Induction of Neuron-Enriched Mitochondrial Proteins Boosts Direct Glia-to-Neuron Conversion

Graphical Abstract

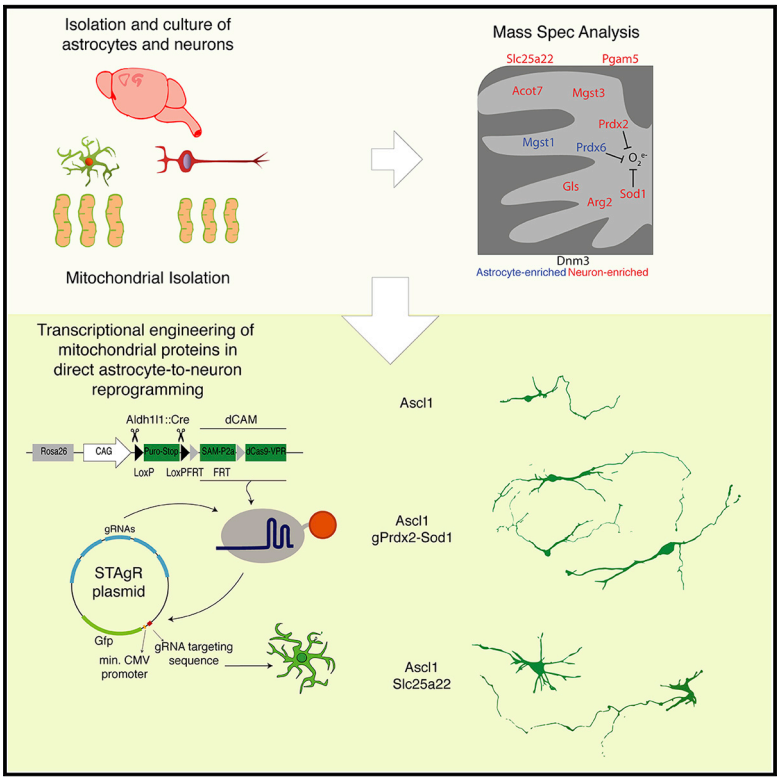

Highlights

- Mitochondrial proteomes of cortical astrocytes and neurons are distinct
- Astrocyte-enriched mitochondrial proteins are downregulated late in neuronal conversion
- Neuron-enriched mitochondrial proteins are upregulated late in neuronal conversion
- Early induction of neuronal mitochondrial proteins improves neuronal reprogramming

Authors

Gianluca L. Russo, Giovanna Sonsalla, Poornemaa Natarajan, ..., Stefanie M. Hauck, Giacomo Masserdotti, Magdalena Götz

Correspondence

magdalena.goetz@helmholtz-muenchen.de

In Brief

Russo et al. identify mitochondrial proteins enriched in neurons or astrocytes. Astrocyte-enriched mitochondrial proteins are often only partially downregulated during astrocyte-to-neuron direct reprogramming. Neuron-enriched ones are upregulated late and mainly in reprogrammed neurons. CRISPRa-mediated early induction of neuron-enriched mitochondrial proteins boosts direct neuronal reprogramming speed and efficiency.

Russo et al., 2021, Cell Stem Cell *28*, 524–534
March 4, 2021
https://doi.org/10.1016/j.stem.2020.10.015

CellPress

CellPress
OPEN ACCESS

Cell Stem Cell

Short Article

CRISPR-Mediated Induction of Neuron-Enriched Mitochondrial Proteins Boosts Direct Glia-to-Neuron Conversion

Gianluca L. Russo,[1,2,3] Giovanna Sonsalla,[1,2,3,15] Poornemaa Natarajan,[1,2,3,15] Christopher T. Breunig,[4,5] Giorgia Bulli,[1,2] Juliane Merl-Pham,[6] Sabine Schmitt,[7] Jessica Giehrl-Schwab,[8] Florian Giesert,[8,9] Martin Jastroch,[10] Hans Zischka,[7,11] Wolfgang Wurst,[8,9,12] Stefan H. Stricker,[4,5] Stefanie M. Hauck,[6,16] Giacomo Masserdotti,[1,2,16] and Magdalena Götz[1,2,13,14,16,*]

[1]Physiological Genomics, Biomedical Center (BMC), Ludwig-Maximilians-Universität (LMU), Planegg-Martinsried, Germany
[2]Institute for Stem Cell Research, Helmholtz Center Munich, BMC LMU, Planegg-Martinsried, Germany
[3]Graduate School of Systemic Neurosciences, BMC, LMU, Planegg-Martinsried, Germany
[4]MCN Junior Research Group, Munich Center for Neurosciences, BMC, LMU, Planegg-Martinsried, Germany
[5]Epigenetic Engineering, Institute of Stem Cell Research, Helmholtz Zentrum, Planegg-Martinsried, Germany
[6]Research Unit Protein Science, Helmholtz Center Munich, Neuherberg, Germany
[7]Institute of Toxicology and Environmental Hygiene, School of Medicine, Technical University Munich (TUM), Munich, Germany
[8]Institute of Developmental Genetics, Helmholtz Center Munich, Neuherberg, Germany
[9]Developmental Genetics, TUM, Munich-Weihenstephan, Germany
[10]Department of Molecular Biosciences, The Wenner-Gren Institute, The Arrhenius Laboratories F3, Stockholm University, Stockholm, Sweden
[11]Institute of Molecular Toxicology and Pharmacology, Helmholtz Center Munich, Neuherberg, Germany
[12]German Center for Neurodegenerative Diseases (DZNE) Site Munich, Munich, Germany
[13]Excellence Cluster of Systems Neurology (SYNERGY), Munich, Germany
[14]Lead Contact
[15]These authors contributed equally
[16]These authors contributed equally
*Correspondence: magdalena.goetz@helmholtz-muenchen.de
https://doi.org/10.1016/j.stem.2020.10.015

SUMMARY

Astrocyte-to-neuron conversion is a promising avenue for neuronal replacement therapy. Neurons are particularly dependent on mitochondrial function, but how well mitochondria adapt to the new fate is unknown. Here, we determined the comprehensive mitochondrial proteome of cortical astrocytes and neurons, identifying about 150 significantly enriched mitochondrial proteins for each cell type, including transporters, metabolic enzymes, and cell-type-specific antioxidants. Monitoring their transition during reprogramming revealed late and only partial adaptation to the neuronal identity. Early dCas9-mediated activation of genes encoding mitochondrial proteins significantly improved conversion efficiency, particularly for neuron-enriched but not astrocyte-enriched antioxidant proteins. For example, Sod1 not only improves the survival of the converted neurons but also elicits a faster conversion pace, indicating that mitochondrial proteins act as enablers and drivers in this process. Transcriptional engineering of mitochondrial proteins with other functions improved reprogramming as well, demonstrating a broader role of mitochondrial proteins during fate conversion.

INTRODUCTION

The ability to regenerate lost neurons after an injury or in neurodegenerative disease is still a key challenge in the field of regenerative medicine. Among different therapeutic approaches (Barker et al., 2018; Grade and Götz, 2017), direct conversion of local glia into neurons has become a viable option to replace functional neurons (Vignoles et al., 2019). Because direct neuronal conversion is dramatically hindered by increased generation of reactive oxygen species (ROS) during the process, Bcl2 or pharmacological application of antioxidants could drastically improve neuronal generation *in vitro* and *in vivo* (Gascón et al., 2016). At the same time, neurons rely on oxidative phosphorylation (OxPhos) (Harris et al., 2012; Herrero-Mendez et al., 2009), so an increase in mitochondrial activity is required during neuronal conversion. Mitochondria perform a plethora of additional functions (Spinelli and Haigis, 2018), and specific mitochondrial proteins may be required to implement the cell-type-specific metabolic needs (Calvo and Mootha, 2010; Folmes et al., 2012; Pagliarini et al., 2008). Because changes in

CellPress
OPEN ACCESS

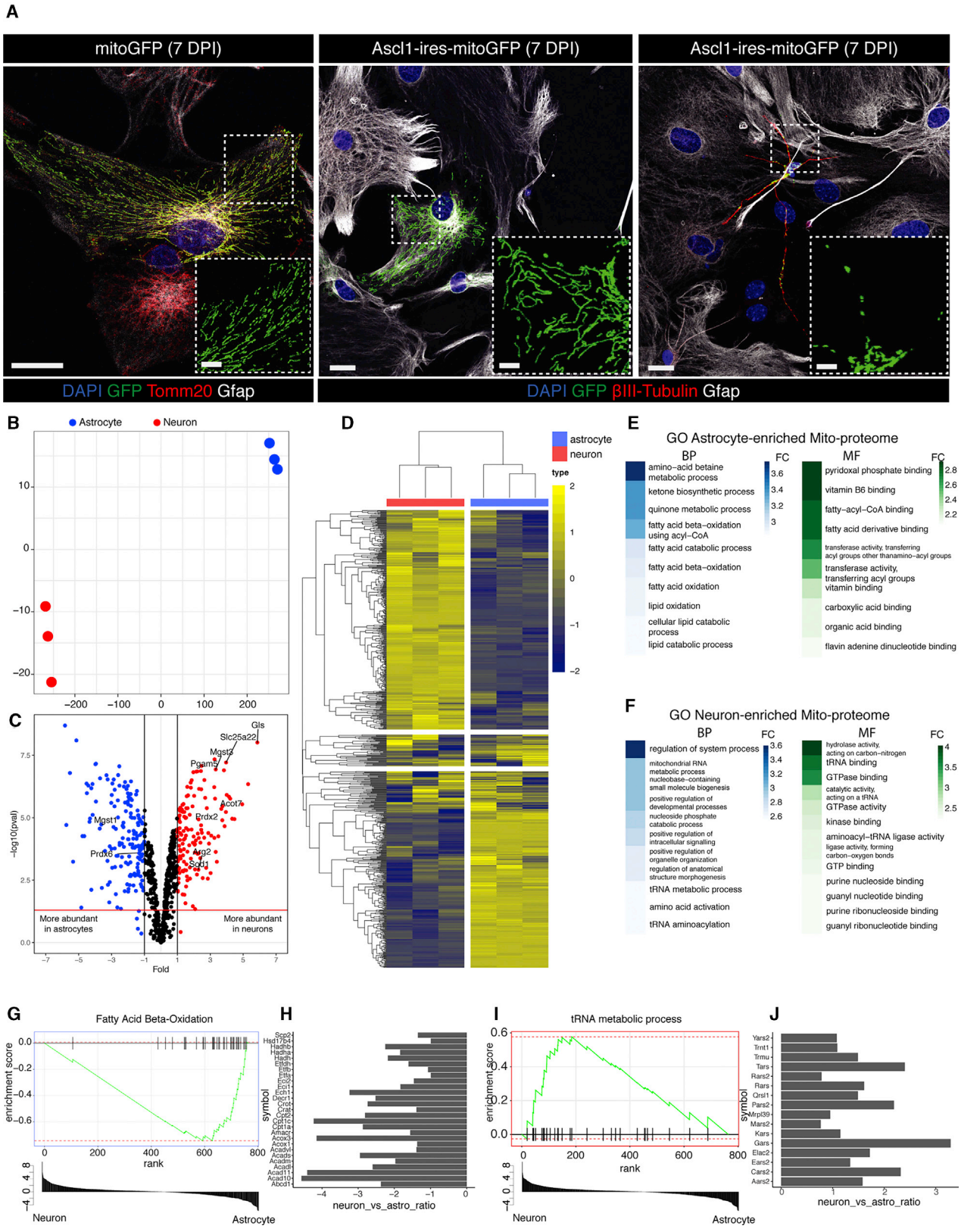

(legend on next page)

mitochondrial proteins have not yet been investigated in neuronal reprogramming, we assessed the similarities and differences in mitochondrial composition for cultured neurons and astrocytes and aimed to improve mismatching during reprogramming by regulating the respective genes by CRISPRa (clustered regularly interspaced short palindromic repeat activation)-mediated transcriptional engineering.

RESULTS

Mitochondrial Morphology Changes during Cortical Astrocyte-to-Neuron Reprogramming *In Vitro*

We first monitored morphological changes of mitochondria during reprogramming. Astrocytes isolated from postnatal day 5 (P5) murine cerebral cortex (Heinrich et al., 2011) were transduced with a retrovirus encoding mitochondrion-targeted green fluorescent protein (*mitoGFP*) with or without the reprogramming proneural factor Achaete-scute homolog 1 (*Ascl1-ires-mitoGFP*, ires [intra ribosome entry site]), shown previously to reprogram astrocytes into GABAergic neurons (Heinrich et al., 2010; Masserdotti et al., 2015). MitoGFP co-localized with Tomm20, a pan-mitochondrial marker protein, revealing an elongated and ramified mitochondrial network in astrocytes (Figure 1A, left panel). This was maintained in Ascl1-transduced astrocytes failing to reprogram (positive for the astroglial protein glia fibrillary acidic protein [Gfap], negative for neuron-specific βIII-tubulin; Figure 1A, center panel), whereas successfully converted neuronal cells (βIII-tubulin+, Gfap−) had smaller mitochondria with shorter and rounder morphology (Figure 1A, right panel). These data are in line with neurons *in vivo* possessing smaller mitochondria and higher fission properties (Misgeld and Schwarz, 2017), whereas astrocytes have more elongated mitochondria and fusion events (Motori et al., 2013). To gain a better understanding of mitochondrial restructuring during the reprogramming process, we investigated the proteins that mediate morphological and functional changes in mitochondria.

Astrocytes and Neurons Differ in Mitochondrial Structure and Function *In Vitro*

To determine the comprehensive mitochondrial proteome of neurons and astrocytes, we chose highly pure neuronal cultures derived from embryonic day 14 (E14) cerebral cortex, cultured for 7 days (Walcher et al., 2013); i.e., young neurons comparable with reprogrammed neurons at 7 days post-transduction (DPT) in reprogramming) and primary cultures of astrocytes as used in direct neuronal reprogramming. Functional bio-energetic differences of neurons and astrocytes from these cultures were confirmed by Seahorse analysis (Figures S1A–S1C). A cell fractionation-based method (Schmitt et al., 2013) enriched mitochondria, as assessed by western blot (Figure S1D) and electron microscopy (EM) (Figure S1E), and functional assays confirmed the isolation of intact mitochondria from both cell types (Figures S1F and S1G). EM confirmed the cell-type-specific differences in mitochondrial morphology (Figures 1A and 1E) and also revealed some other organelles in the neuronal samples, probably because small mitochondria are tightly linked to the cytoskeleton in the thin neuronal processes and the endoplasmic reticulum (ER) (Fecher et al., 2019).

Astrocytes and Neurons Exhibit Profound Differences in Their Mitochondrial Proteome

We then used liquid chromatography-tandem mass spectrometry (LC-MS/MS) to identify proteins in neuronal and astrocytic mitochondria. A *t*-distributed stochastic neighbor embedding (t-SNE) plot for all identified proteins normalized for abundance (Figures S1J; normalization in Figure S1H) or mitochondrion-specific proteins (Figure 1B; normalization in Figure S1K), as classified by MitoCarta 2.0 (Table S1; Calvo et al., 2016), revealed clear separation of neurons and astrocytes. Unsupervised cluster analysis confirmed the cell type dependent similarity, considering whole proteins (Figure S1I) or only mitochondrial proteins (Figure S1L). Overall, we detected 757 (±1) mitochondrial proteins in astrocytes and 738 (±1) in neurons (Figures S1M and S1N) of which 164 (22%) were more abundant in astrocytes and 141 (19%) more abundant in neurons ($p < 0.05$ and 2-fold enrichment; Figure 1C; Table S1), with high reproducibility across samples (Figure 1D). Thus, about a fifth of the mitochondrial proteome differs significantly between these cell types. Western blotting of whole-cell lysates from independent cultures confirmed enrichment of Sfxn5 and Cpox in astrocytes (Figure S1O, left and center panel) and glutaminase (Gls) in neurons (Figure S1O, right panel).

Gene Ontology (GO) term analysis of mitochondrial proteins significantly enriched in astrocytes (Figure 1E, left panel; top 10 enriched biological processes [BPs]; Fisher's exact test < 0.01; see Table S2A for a complete list) revealed terms such as fatty acid catabolic process, fatty acid β-oxidation, and lipid catabolic process, also relevant pathways for astrocytes *in vivo* (van Deijk et al., 2017). This was supported by the analysis of molecular function (MF) GO terms (Figure 1E, right panel; Table

Figure 1. Astrocytes and Neurons Differ in Mitochondrial Structure and Proteome

(A) Micrograph of mitochondrial morphology in control (mitoGFP) astrocytes (left panel), Ascl1-non-reprogrammed astrocytes (center panel), and Ascl1-induced neurons (right panel, Ascl1-mitoGFP), 7 DPI. Scale bars, 20 μm and 6 μm (insets).

(B) *t*-SNE plot of samples considering only mitochondrial proteins.

(C) Volcano plot of mitochondrial proteins with $\log_2$ ratio of abundance of neurons/astrocytes (x axis) and the $-\log_{10}$ of the corresponding significance value (p value, y axis); 2-fold changes (vertical lines), significance cutoff p = 0.05 (horizontal line). Proteins significantly more abundant in astrocytes are shown in blue and more abundant in neurons in red. Names highlight proteins covered in this study.

(D) Unsupervised heatmap cluster analysis of all detected mitochondrial proteins. Astrocytes, blue; neurons, red. n = 3 for each group. The color scale indicates *Z* score.

(E and F) GO terms of the top 10 biological processes (BPs; blue, left panels) and molecular functions (MFs; green, right panels) for astrocyte-enriched (E) and neuron-enriched (F) mitochondrial proteins. The color bar represents the fold change compared with the expected number of genes for each term. Terms were considered if exact Fisher test < 0.01.

(G–J) Examples of 2 terms identified by gene set enrichment analysis (GSEA) (G and I) and barplots (H and J) of the main genes associated with the respective terms (in G or I).

S2A), including terms such as fatty-acyl-coenzyme A (CoA) binding, in line with a recent study of mitochondria of Bergmann glia from adult mice (Fecher et al., 2019). Likewise, gene set enrichment analysis (GSEA) identified fatty acid β-oxidation-related proteins in astrocytes (Figure 1G; Table S2E), comprising key regulators such as Acads, Cpt1a, and Cpt2 (Figure 1H; Tables S1 and S2E).

To explore the functional relevance of the fatty acid β-oxidation pathway in direct reprogramming, we blocked this pathway using etomoxir, an inhibitor of Cpt1a (Jernberg et al., 2017), early during the conversion process (Figure S2A). Medium to high doses of etomoxir (25 μM and 100 μM, respectively) improved reprogramming compared to the control (no etomoxir) upon Ascl1 (Figures S2B and S2C) or Neurogenin2 (Neurog2) expression (Figures S2D and S2E). Interestingly, co-treatment with α-tocotrienol, an analog of the ROS scavenger vitamin E, reduced Ascl1-mediated reprogramming efficiency, suggesting that the positive effect of etomoxir might be partly due to an increase in ROS, as shown previously (O'Connor et al., 2018). Thus, β-oxidation is a general hurdle in glia-to-neuron reprogramming.

GO terms significant for neuron-enriched mitochondrial proteins were associated with RNA metabolism and function (BP in Figure 1F, left panel, and Table S2C; MF in Figure 1F, right panel, and Table S2D) and further supported by GSEA (Figures 1I and 1J, tRNA metabolic process; full list in Table S2E). This highlights the notion that tRNA biogenesis is an important activity in neuronal mitochondria and its dysfunction is associated with neurodevelopmental disease (Schaffer et al., 2019). Among neuron-enriched mitochondrial proteins, we also detected Gls, the enzyme regulating glutamine metabolism and glutamate neurotransmitter levels (Márquez et al., 2009), and ATP citrate lysate (Acly), involved in production of cytosolic acetyl-CoA (Lin et al., 2013; Table S1).

Enrichment of the mitochondrial fusion protein Mitofusin 1 (Mfn1) in astrocytes is in line with the presence of more elongated mitochondria in such cells (Figure 1A), whereas the fission master regulator Dynamin-related protein (Dnm1l, also known as Drp1) is more prevalent in the neuronal mitochondrial proteome (Table S1). Interestingly, the antioxidant proteins Gpx1, Gpx4, Prdx6, and Mgst1 were more enriched in astrocytes (Table S1), whereas Mgst3, Prdx2, and Sod1 were more abundant in neurons (Table S1), suggesting that different members of antioxidant protein families (e.g., peroxiredoxins and microsomal glutathione S-transferases) are enriched in specific cell types. This raised the intriguing question of whether these proteins (Prdx2 and Prdx6 or Mgst1 and Mgst3) are functionally similar and only expressed in a cell-type-specific manner or whether the neuron-enriched antioxidant proteins may be specifically required in neurons and, hence, during the direct conversion process.

We also compared our data with mitochondrial proteins isolated from adult murine cerebellum (Purkinje cells, granule cells, and astrocytes; Fecher et al., 2019). Despite the very different experimental conditions (*in vivo* versus *in vitro*, adult versus postnatal, cerebellum versus cortex, immunoprecipitation [IP]-based versus fractionation-based-method), we found 117 proteins enriched in both astrocyte-derived samples; i.e., 60% of all mitochondrial proteins identified by Fecher et al. (2019) were also present in our astrocyte-enriched mitochondrial proteome (Figure S1P). Likewise, 46% of neuron-enriched mitochondria identified by Fecher et al. (2019) were common to our neuronal dataset (Figure S1Q).

Thus, the mitochondrial proteome already differs profoundly in astrocytes and neurons *in vivo* and *in vitro*, comprising broad categories of protein functions from metabolism to tRNA synthesis and mitochondrial translation.

Mitochondrial Protein Changes during Astrocyte-to-Neuron Reprogramming

To determine whether and when astrocytes downregulate their characteristic mitochondrial proteins and express neuron-enriched ones during reprogramming, we chose differentially enriched functionally relevant candidates detectable by immunostaining (Table S1). The immunofluorescence intensity of the candidates was quantified and normalized to the signal intensity of the pan-mitochondrial protein Tomm20, preventing any bias of the total mitochondrial mass on quantification.

Sfxn5, a mitochondrial transporter of citrate (Miyake et al., 2002), an essential intermediate of the tricarboxylic acid cycle (TCA), was enriched in astrocyte-derived mitochondria (Table S1). Accordingly, its level was much higher in astrocytes or DsRed-transduced controls than in reprogrammed neurons (Figures 2A, 2B, and 2D). During *Ascl1*-mediated reprogramming, Sfxn5 was similar to control astrocytes at early stages (Figures 2A and 2D), whereas βIII-tubulin+ reprogrammed neurons had significantly lower levels (Figures 2B and 2D). Notably, Sfxn5 and Tomm20 showed a greater colocalization in *Ascl1*-transduced cells at 1 than 7 DPT (Figure 2C), supporting the notion that Sfxn5 is mitochondrially localized in astrocytes and disappears in induced neurons (iNeurons). Likewise, the astrocyte-enriched mitochondrial protein Cpox (Mori et al., 2013), highly expressed in astrocytes (Figures S3A, S3B, and S3D) was downregulated significantly in Ascl1-transduced cells (Figures S3B and S3D, center panel), but to a lower degree in *Ascl1*-transduced astrocytes than in *Ascl1*-iNeurons (Figures S3C and S3D). These data show a relatively late (5–7 DPT) regulation of Sfxn5 and Cpox. The lack of downregulation in reprogramming-resistant astrocytes prompts the suggestion that this may contribute to failure of reprogramming.

Among neuron-enriched mitochondrial proteins, we examined Prdx2, which catalyzes the reduction of peroxides and, hence, protects against oxidative stress (Boulos et al., 2007). Prdx2 was not detected in astrocytes (Figures 2E, 2F, and 2H), while *Ascl1*-transduced cells had some Prdx2 signal at 3 DPT, with the strongest increase at 5–7 DPT in *Ascl1*-iNeurons (Figures 2F and 2H). At 7 DPT, Prdx2 reached a level similar to that observed in primary neurons (Figure 2H) and co-localized with Tomm20 (Figure 2G). Similarly, Gls, fundamental for glutamate production and glutamate and GABA transmitter levels as well as neuronal differentiation (Velletri et al., 2013), showed the strongest expression in iNeurons (5–7 DPT; Figures S3F and S3H), where it colocalized with Tomm20 (Figure S3G). Notably, its upregulation started earlier, at 1 DPT (Figure S3H), but did not reach the levels of primary cortical neurons (Figure S3H, right panel).

Mitochondrial proteins enriched in astrocytes (Sfxn5 and Cpox) or neurons (Prdx2 and Gls) change relatively late during

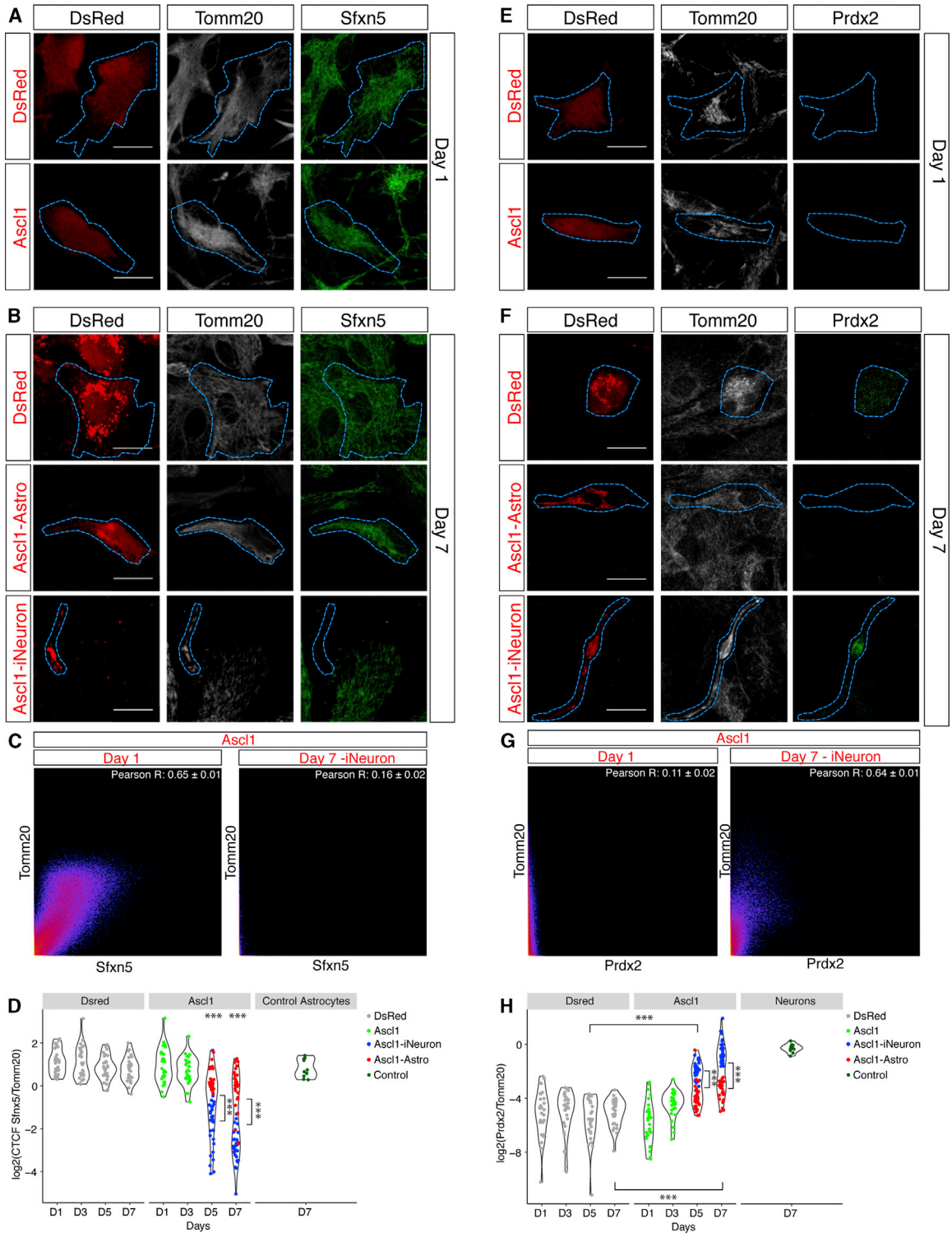

Figure 2. Mitochondrial Protein Changes during Astrocyte-to-Neuron Reprogramming

(A, B, E, and F) Micrographs showing immunostaining in astrocytes transduced with DsRed or Ascl1-ires-DsRed as indicated. Scale bars, 20 μm.

(C and G) Examples of scatterplots of the pixel intensity correlation between Tomm20 and Sfxn5 (C) or Prdx2 (G) in Ascl1-transduced cells on day 1 (left panel) and in reprogrammed cells on day 7 (right panel). Pearson's coefficient as average of 3 cells/biological replicate; n = 3 biological replicates.

(D and H) Violin plots of the $\log_2$ ratio of the intensity of the expression of Sfxn5 (D) or Prdx2 (H) normalized to Tomm20 intensity over time. Each dot represents 1 cell. 10 cells analyzed/biological replicate/condition/day. n = 3 biological replicates; ***$p \leq 0.001$.

CellPress
OPEN ACCESS

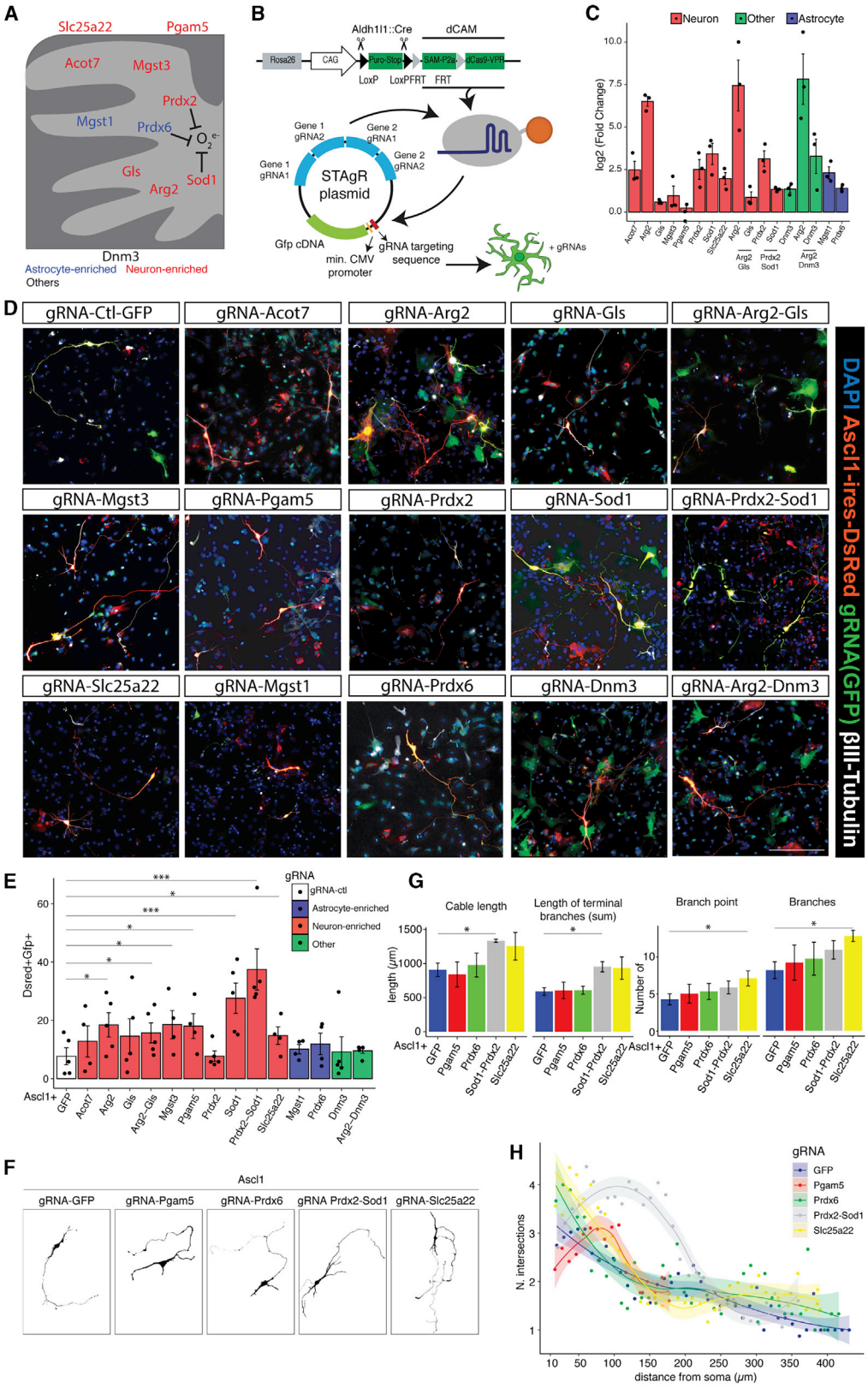

(legend on next page)

neuronal reprogramming. Remarkably, the changes correlated with the degree of conversion, prompting the hypothesis that they may be functionally relevant.

CRISPRa-Mediated Induction of Neuron-Enriched Mitochondrial Proteins Improves the Efficiency of Direct Neuronal Reprogramming

To test the above prediction, we chose 8 candidates enriched in neuronal mitochondria (Figures S4A and S4B; Table S1; Fecher et al., 2019): Sod1 and Prdx2 for their antioxidant activity in neurons (Liu et al., 2020; Rosen, 1993), acyl-CoA thioesterase 7 (Acot7), arginase 2 (Arg2), Gls, microsomal Gst3 (Mgst3), mitochondrial serine/threonine protein phosphatase (Pgam5), and solute carrier 25 member 22 (Slc25a22) (Figure 3A). Among astrocyte-enriched antioxidant mitochondrial proteins, we selected Prdx6 (Fisher, 2011) and the microsomal glutathione S-transferase Mgst1, a member of the membrane-associated proteins in eicosaonid and glutathione metabolism (MAPEG) family, as Mgst3 (Bresell et al., 2005). Dynamin 3 (Dnm3) was included as a protein with mitochondrion-unrelated functions (Gu et al., 2010; Figure 3A).

Quantitative RT-PCR from cells isolated by fluorescence-activated cell sorting (FACS) 48 h after transfection of the dCas9-VPR coding plasmid (Breunig et al., 2018b) and non-targeting control gRNAs or gRNAs designed to target the promoter region of the above candidates showed different levels of induction (Figure 3C; *Arg2*, ~94-fold; *Acot7*, *Prdx2*, *Sod1*, *Slc25a22*, *Dnm3*, *Mgst1*, and *Prdx6*, ~ 5-fold; *Gls*, *Mgst3*, and *Pgam5*, ~2-fold). Multiple gRNAs targeting different genes (e.g., Arg2+-Gls) did not alter the induction levels of their specific targets, and no significant induction was detectable for six putative off targets of each gRNA (Figure S4C).

gRNAs for the selected candidates were cloned in a plasmid with a GFP reporter module whose activation depends on the presence of the self-transcribed gRNAs (e.g., for Sod1) and dCas9-CAM (Figure 3B). Then, primary cultures of astrocytes, obtained by crossing a transgenic mouse line in which the dCas9 gene is fused to three transactivating domains (VP64, p65, and RTA[R transactivator]) and SAM (synergistic activator Mediator) components (dCAM) (Chavez et al., 2015; Konermann et al., 2015; STAR Methods) with the astrocyte-specific Aldh1l1:-Cre mouse line (Tien et al., 2012; Figure 3B), were co-transfected with the constructs for *Ascl1-ires-DsRed* and the control STAgR-GFP (*gRNA-GFP*) or gene-specific gRNA, and neuronal conversion was examined 8 DPT. Strikingly, the induction of many, but not all, genes coding for neuron-enriched mitochondrial proteins improved the reprogramming efficiency (Figures 3D and 3E). Induction of *Sod1* resulted in the highest reprogramming efficiency alone or in combination with *Prdx2* (Figure 3D and 3E; Figure S4D). In addition, induction of *Arg2* and *Mgst3* as well as *Pgam5* and *Slc25a22*, which do not have any reported antioxidant activity, significantly improved the conversion efficiency (Figures 3D and 3E). Remarkably, the induction of genes coding for astrocyte-enriched mitochondrial proteins, even with antioxidant function (*Mgst1* and *Prdx6*), was not beneficial for reprogramming, like *Dnm3* (Figures 3D and 3E). This highlights the need for neuron-enriched antioxidants (e.g., Sod1 and Mgst3) and shows that members of the same family (e.g., Mgst1 and Mgst3) are clearly not functionally redundant. The expression of neuron-enriched candidates also resulted in a more complex morphology of iNeurons, with more neurite outgrowth in Ascl1-Sod1+Prdx2-co-expressing neurons and more branches in Ascl1-Slc25a22-co-expressing neurons (Figures 3F and 3G).

These data suggest that neuron-specific mitochondrial proteins are particularly important during the conversion process and that their earlier and/or higher expression improves reprogramming.

CRISPRa-Mediated Induction of Prdx2 and Sod1 Improves Neuronal Reprogramming by Faster Conversion into Neurons with a Longer Lifespan

To investigate the effect of the early activation of mitochondrial proteins on neuronal conversion, we followed single cells by live imaging as described before (Costa et al., 2011), from 28 h after the transfection for 6 days with GFP/DsRed pictures taken every 4 h (Figure 4A; Figure S2F; Video S1). *Ascl1-Prdx2-Sod1*-co-transfected cells with neuron-like morphology (smaller cell soma and processes longer than 3× the soma length; Gascón et al., 2016) were already increased significantly at 75 h compared with *Ascl1*-only cells (Figure 4B). *Prdx2* and *Sod1* co-activation significantly increased the lifespan of all tracked cells (Figure 4C), mainly because of an increased lifespan of the converted neurons (Figures 4E and 4F), but not of non-reprogrammed astrocytes (Figure 4D), consistent with the cell-type-specific role of antioxidants. Measuring the conversion speed (when cells first acquire a neuron-like morphology) showed a bi-phasic distribution in *Ascl1*-transfected cells (Figure 4G). Cells turning into neurons fast (red dots) typically died before the end of the experiment, whereas those that reprogrammed at a slower pace (blue dots) survived until the end of the video session at 6 DPT (Figure 4G). This was remarkably different in *Ascl1-Prdx2-Sod1*-expressing cells: many cells

Figure 3. CRISPRa-Mediated Activation of Neuron-Enriched Mitochondrial Proteins Improves Neuronal Reprogramming

(A and B) Schemes of the selected candidates in mitochondria and the dCas9-CAM-STAgR (string assembly gRNA) system employed here.

(C) Real-time quantitative PCR (qPCR) of the candidates in dCas9-CAM gene-specific gRNA-expressing cells. Data are shown as $\log_2$ fold change over the gRNA scramble control (mean ± SEM). n = 3 for each group.

(D) Micrographs showing reprogrammed cells (βIII-tubulin$^+$-DsRed$^+$-GFP$^+$) upon co-transfection of Ascl1-ires-DsRed (red) and different STAgR constructs (green). Scale bar, 100 μm.

(E) Reprogramming efficiency as the percentage of βIII-tubulin$^+$/DsRed$^+$/GFP$^+$ at 7 DPT. Data are shown as mean ± SEM. *p < 0.05, ***p < 0.001. n = 5 per experimental condition.

(F) Examples of the morphology of reprogrammed neurons co-expressing Ascl1 and the indicated gRNAs.

(G) Morphological analysis of reprogrammed neurons upon induction of selected candidates (x axis). Data are shown as mean ± SEM. Paired t test, *p ≤ 0.05; n = 4 biological replicates.

(H) Sholl analysis of reprogrammed neurons co-expressing Ascl1 and the indicated candidates. Data are shown as mean ± SEM. Paired t test, *p ≤ 0.05; n = 4 biological replicates.

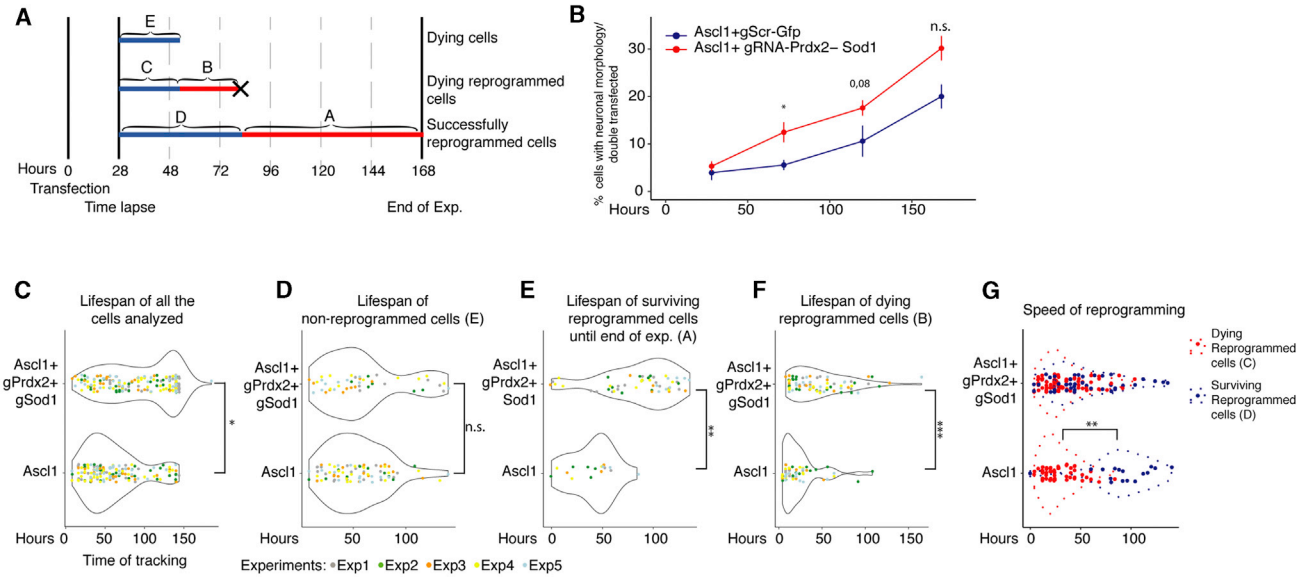

Figure 4. Continuous Single-Cell Live Imaging Reveals Several Roles of Prdx2-Sod1 Activation in Neuronal Reprogramming

(A) Scheme of continuous live imaging and the analysis performed.

(B) Time course analysis of the percentage of cells acquiring neuronal morphology over double-transfected cells at the indicated time points. Data are shown as mean ± SEM. *p ≤ 0.05. n = 3 biological replicates for each group.

(C and D) Violin plot showing the lifespan of all cells analyzed irrespective of their final identity (C) and cells that died without converting (D), following expression of *Ascl1-gRNA-GFP* or *Ascl1-gRNA-Prdx2-Sod1*. n = 5 biological replicates for each group. *p ≤ 0.05

(E–G) Violin plots showing the lifespan (E and F) and speed of reprogramming (G) upon expression of *Ascl1-gRNA-GFP* or *Ascl1-gRNA-Prdx2-Sod1*. n = 5 biological replicates (color-coded) for each group. *p ≤ 0.05, **p ≤ 0.01, ***p ≤ 0.001.

reprogrammed fast and survived until the end of the experiment (Figure 4G). Importantly, this is not due to improved survival of the fast-converting cells that would die under the *Ascl1*-only condition because a similar number of cells converting fast and dying (blue dots and curve in Figure 4G) was observed among *Ascl1-Prdx2-Sod1* cells. Rather, many more cells were recruited for reprogramming under the *Ascl1-Prdx2-Sod1* condition and in a fast manner (Figure 4G). We therefore conclude that activation of these neuron-enriched mitochondrial proteins speeds up the conversion process in addition to its role in protecting neurons from cell death.

DISCUSSION

Here we describe the comprehensive mitochondrial proteomes of cortical astrocytes and neurons that show quantitative differences in a fifth of the identified proteins. The functional relevance of these differences is shown by the fact that cells failing to upregulate neuron-enriched mitochondrial proteins often do not reprogram; activating their expression improved the reprogramming efficiency, and astrocyte-enriched mitochondrial proteins, even with known antioxidant function, have no such effects.

Astrocyte Metabolism and Its Influence on Neuronal Reprogramming

Astrocytes share similarities with neural stem cells (NSCs) (Götz et al., 2015). For example, we and others (Fecher et al., 2019) found the mitochondrial proteome of astrocytes to be enriched for the GO terms lipid metabolism and fatty acid β-oxidation, also highly represented in neural stem cells (NSCs) and downregulated during adult neurogenesis (Knobloch et al., 2017; Llorens-Bobadilla et al., 2015). Despite the fast transcriptional changes at early stages of reprogramming (Gascón et al., 2016; Masserdotti et al., 2015), genes associated with lipid metabolism (e.g., *Cpt1a*) are not yet downregulated after 48 h (Gascón et al., 2016; Masserdotti et al., 2015), suggesting slow metabolic conversion, a limiting factor in induced pluripotent stem cell (iPSC) reprogramming (Wu et al., 2016). Accordingly, etomoxir-mediated reduction of fatty acid β-oxidation improved neuronal reprogramming (Figure S3), indicating that the manipulation of specific metabolic pathways might substantially contribute to remove hurdles during the conversion. The addition of ROS scavenger reduced the reprogramming efficiency combined with etomoxir, suggesting potential beneficial effects of ROS under this condition. It will be interesting to determine the level of ROS above which it shows deleterious effects.

Early Activation of Neuron-Enriched Mitochondrial Proteins with a Wide Functional Spectrum Improves Astrocyte-to-Neuron Conversion

The comprehensive mitochondrial proteome revealed cell-type-specific enrichment of antioxidant proteins; e.g., Mgst1 and Mgst3 were enriched in the mitochondrial proteome of astrocytes and neurons, respectively. Remarkably, early CRISPRa-mediated induction of the latter, but not the former, improved direct neuronal conversion, demonstrating the key functional role of cell-type-specific but similar antioxidant proteins. Sod1 activation had the most potent effect, in line with its functional relevance in neurodegeneration (Kaur et al., 2016). However, other mitochondrial proteins with antioxidant functions, such

as Prdx6 and Prdx2 (enriched in astrocytes and neurons, respectively) did not improve reprogramming, showing that only some antioxidants perform highly cell-type-specific functions relevant in direct neuronal reprogramming.

The early activation of neuron-enriched mitochondrial proteins without any reported antioxidant activity also significantly increased direct reprogramming efficiency. Pgam5, a mitochondrial phosphatase that associates with the RIP1/RIP3/MLKL (Mixed lineage kinase domain-like pseudokinase) complex, doubled *Ascl1*-induced reprogramming efficiency, possibly by inhibiting necroptosis (Gascón et al., 2016; Lu et al., 2016). In addition, Pgam5 regulates mitochondrial homeostasis and dynamics by dephosphorylating Drp1, BCL-xL (B-cell lymphoma extra large), and FUNDC1 (Ma et al., 2020), a key process for neuronal function and survival (Lu et al., 2014). Likewise, the mitochondrial glutamate transporter Slc25a22, which also improved reprogramming by 2-fold, is important for brain function (Cohen et al., 2014; Molinari et al., 2005, 2009; Poduri et al., 2013) by regulating glutamate levels (Goubert et al., 2017).

Conversely, the activation of Gls did not significantly improve reprogramming, suggesting that glutamate biogenesis does not have a major role in this process. Likewise, the activation of a non-mitochondrial protein, Dnm3, expressed at similar levels in astrocytes and neurons, had no effect. These results confirm our cutoff criteria and highlight a potent role of only some neuron-enriched mitochondrial proteins in direct conversion by influencing several functional pathways.

Notably, astrocyte-enriched mitochondrial proteins, like Sfnx5 and Cpox, were only partially downregulated in reprogramming and maintained a higher expression in cells that failed to convert. This indicates that these cells face a "confused" metabolic state that may hinder reprogramming and highlights the importance to further ease the metabolic transition for proper conversion. Indeed, "on-memory" genes not shut off during reprogramming from the original starter cell limit the conversion process (Hormanseder et al., 2017).

Neuron-Enriched Mitochondrial Protein Activation as an Enabler and Driver in Reprogramming

Most improvement in reprogramming efficiency was achieved by early expression of the neuron-enriched mitochondrial proteins Sod1 and Prdx2: they increased recruitment of more cells into the conversion process and improved survival only of reprogrammed neurons and their differentiation. Thus, early activation of these neuron-enriched mitochondrial antioxidants protects neurons, but not astrocytes, against aberrant ROS levels (Gascón et al., 2016).

Remarkably, *Ascl1*-expressing cells showed a significant difference in conversion speed between neurons that survive and those that do not survive for 6 days, with the former converting much slower. This is reminiscent of natural neurogenesis, where the transition from progenitors to neurons often occurs more gradually via intermediate progenitors (Khacho et al., 2016; Llorens-Bobadilla et al., 2015), suggesting the need for a period of adaptation to support the new identity. Surprisingly, the expression of *Prdx2* and *Sod1* speeds up the conversion process in cells surviving until the end of the time lapse, similarly to co-expression of Bcl2 (Gascón et al., 2016). Thus, different mitochondrion-dependent pathways may speed up the conversion rate by improving cell survival and/or protecting against ROS damage. We therefore propose that failure or late activation of neuron-enriched mitochondrial proteins may impair the conversion process at several levels, ultimately causing cells to die. Importantly, this occurs despite the expression of a multitude of antioxidant and metabolic proteins present in astrocytes. Thus, direct neuronal reprogramming sheds new light on the function of cell-type-enriched mitochondrial proteins.

Limitations of Study

Clearly, it would be desirable to follow the mitochondrial proteome in a comprehensive manner during the reprogramming process, which will be made easier by newly developed mouse lines with tagged mitochondrial proteins (Fecher et al., 2019), also in the murine brain *in vivo* or human cells *in vitro*. Ideally, these could be compared with fully differentiated neurons; here we choose culture conditions and time points to match the reprogramming protocol.

STAR★METHODS

Detailed methods are provided in the online version of this paper and include the following:

- KEY RESOURCES TABLE
- RESOURCE AVAILABILITY
  - Lead Contact
  - Materials Availability
  - Data and Code Availability
- EXPERIMENTAL MODEL AND SBJECT DETAILS
  - Wild-type mice (Primary Cell culture, Proteomics, IHC)
  - Aldh1-Cre and Cre-inducible dCas9-VPR mice
  - Primary cultures of cortical astrocytes
  - Cells undergoing direct neuronal conversion
  - Primary cultures of cortical neurons
- METHOD DETAILS
  - Transfection and Transduction
  - Fluorescence-activated Cell Sorting
  - Mitochondria isolation
  - Characterization of isolated mitochondria
  - Seahorse experiments
  - Proteome analysis
  - Western Blot Analysis
  - Immunocytochemistry
  - RNA extraction, retro-transcription and Real Time Quantitative PCR (qRT-PCR)
  - STAgR cloning
  - Live-Imaging Microscopy
- QUANTIFICATION AND STATISTICAL ANALYSIS

SUPPLEMENTAL INFORMATION

Supplemental Information can be found online at https://doi.org/10.1016/j.stem.2020.10.015.

ACKNOWLEDGMENTS

Particular thanks go to Caroline Fecher and Thomas Misgeld (Technical University of Munich) for providing the antibodies against Sfxn5 and Gls and sharing their proteome data and expertise about mitochondria. We are very

grateful to Tatiana Simon (BMC, Munich) and Andrea Steiner-Mezzadri (Helmholtz Center Munich) for technical assistance, Daniel Brandt for technical support with the Seahorse analyzer, Uli Ohmayer for initial proteomic analysis, Andreas Beyerlein and Hannah Busen from Core Facility Statistical Consulting (all from Helmholtz Center Munich), Tobias Straub (Bioinformatic Core Facility of the BMC, LMU, Munich) and Pawel Smialowski (Helmholtz Zentrum, Munich) for help with R coding, Tamas Schauer for advice regarding DHARMa, and Nicola Mattugini for comments on the manuscript. This work was funded by the Fondation Rodger de Spoelberch, the German Research Foundation (SFB870 and SPP1757), the advanced ERC ChroNeuroRepair and ERAnet (to M.G.), SPP2127 (to S.M.H.), and ExNet-0041-Phase2-3 (SyNergy-HMGU) and AMPro Project (Aging and Metabolic Programming) network funds of the Helmholtz Association (to W.W.).

AUTHOR CONTRIBUTIONS

M.G. conceived and designed the project. G.L.R. and G.M. shaped the project, and G.L.R. performed experiments and analysis. G.S. contributed to the time course analysis. P.N. performed and analyzed the experiment with etomoxir, gRNA, and continuous live imaging. C.T.B. and S.H.S. provided CRISPR-Cas expertise and developed and designed the STAgR approach, and C.T.B. helped with cloning of the constructs. G.B. performed western blots. J.M.-P. and S.M.H. provided proteomics expertise and performed experiments and analysis. S.S. and H.Z. performed mitochondrial isolation and electron microscopy. J.G.-S., F.G., and W.W. generated and provided dCAM transgenic mice. M.J. provided expertise regarding metabolism and Seahorse analysis. G.M. analyzed the data; provided expertise and training of G.L.R., G.S., P.N., and G.B. regarding reprogramming; and co-directed the project together with M.G. G.L.R., G.M., and M.G. wrote the manuscript, and all authors contributed corrections and comments.

DECLARATION OF INTERESTS

The authors declare no competing interests.

Received: August 5, 2019
Revised: August 11, 2020
Accepted: August 20, 2020
Published: November 16, 2020; corrected online: December 2, 2020

REFERENCES

Barker, R.A., Götz, M., and Parmar, M. (2018). New approaches for brain repair-from rescue to reprogramming. Nature *557*, 329–334.

Boulos, S., Meloni, B.P., Arthur, P.G., Bojarski, C., and Knuckey, N.W. (2007). Peroxiredoxin 2 overexpression protects cortical neuronal cultures from ischemic and oxidative injury but not glutamate excitotoxicity, whereas Cu/Zn superoxide dismutase 1 overexpression protects only against oxidative injury. J. Neurosci. Res. *85*, 3089–3097.

Bresell, A., Weinander, R., Lundqvist, G., Raza, H., Shimoji, M., Sun, T.H., Balk, L., Wiklund, R., Eriksson, J., Jansson, C., et al. (2005). Bioinformatic and enzymatic characterization of the MAPEG superfamily. FEBS J. *272*, 1688–1703.

Breunig, C.T., Durovic, T., Neuner, A.M., Baumann, V., Wiesbeck, M.F., Köferle, A., Götz, M., Ninkovic, J., and Stricker, S.H. (2018a). One step generation of customizable gRNA vectors for multiplex CRISPR approaches through string assembly gRNA cloning (STAgR). PLoS ONE *13*, e0196015.

Breunig, C.T., Neuner, A.M., Giehrl-Schwab, J., Wurst, W., Götz, M., and Stricker, S.H. (2018b). A Customizable Protocol for String Assembly gRNA Cloning (STAgR). J. Vis. Exp. (142), e58556.

Calvo, S.E., and Mootha, V.K. (2010). The mitochondrial proteome and human disease. Annu. Rev. Genomics Hum. Genet. *11*, 25–44.

Calvo, S.E., Clauser, K.R., and Mootha, V.K. (2016). MitoCarta2.0: an updated inventory of mammalian mitochondrial proteins. Nucleic Acids Res. *44* (D1), D1251–D1257.

Chavez, A., Scheiman, J., Vora, S., Pruitt, B.W., Tuttle, M., P R Iyer, E., Lin, S., Kiani, S., Guzman, C.D., Wiegand, D.J., et al. (2015). Highly efficient Cas9-mediated transcriptional programming. Nat. Methods *12*, 326–328.

Cohen, R., Basel-Vanagaite, L., Goldberg-Stern, H., Halevy, A., Shuper, A., Feingold-Zadok, M., Behar, D.M., and Straussberg, R. (2014). Two siblings with early infantile myoclonic encephalopathy due to mutation in the gene encoding mitochondrial glutamate/H+ symporter SLC25A22. Eur. J. Paediatr. Neurol. *18*, 801–805.

Costa, M.R., Ortega, F., Brill, M.S., Beckervordersandforth, R., Petrone, C., Schroeder, T., Götz, M., and Berninger, B. (2011). Continuous live imaging of adult neural stem cell division and lineage progression in vitro. Development *138*, 1057–1068.

Fecher, C., Trovò, L., Müller, S.A., Snaidero, N., Wettmarshausen, J., Heink, S., Ortiz, O., Wagner, I., Kühn, R., Hartmann, J., et al. (2019). Cell-type-specific profiling of brain mitochondria reveals functional and molecular diversity. Nat. Neurosci. *22*, 1731–1742.

Ferreira, T.A., Blackman, A.V., Oyrer, J., Jayabal, S., Chung, A.J., Watt, A.J., Sjöström, P.J., and van Meyel, D.J. (2014). Neuronal morphometry directly from bitmap images. Nat. Methods *11*, 982–984.

Fisher, A.B. (2011). Peroxiredoxin 6: a bifunctional enzyme with glutathione peroxidase and phospholipase A_2 activities. Antioxid. Redox Signal. *15*, 831–844.

Folmes, C.D., Dzeja, P.P., Nelson, T.J., and Terzic, A. (2012). Metabolic plasticity in stem cell homeostasis and differentiation. Cell Stem Cell *11*, 596–606.

Gascón, S., Murenu, E., Masserdotti, G., Ortega, F., Russo, G.L., Petrik, D., Deshpande, A., Heinrich, C., Karow, M., Robertson, S.P., et al. (2016). Identification and Successful Negotiation of a Metabolic Checkpoint in Direct Neuronal Reprogramming. Cell Stem Cell *18*, 396–409.

Gibson, D.G. (2011). Enzymatic assembly of overlapping DNA fragments. Methods Enzymol. *498*, 349–361.

Götz, M., Sirko, S., Beckers, J., and Irmler, M. (2015). Reactive astrocytes as neural stem or progenitor cells: In vivo lineage, In vitro potential, and Genome-wide expression analysis. Glia *63*, 1452–1468.

Goubert, E., Mircheva, Y., Lasorsa, F.M., Melon, C., Profilo, E., Sutera, J., Becq, H., Palmieri, F., Palmieri, L., Aniksztejn, L., and Molinari, F. (2017). Inhibition of the Mitochondrial Glutamate Carrier SLC25A22 in Astrocytes Leads to Intracellular Glutamate Accumulation. Front. Cell. Neurosci. *11*, 149.

Grade, S., and Götz, M. (2017). Neuronal replacement therapy: previous achievements and challenges ahead. NPJ Regen. Med. *2*, 29.

Gu, C., Yaddanapudi, S., Weins, A., Osborn, T., Reiser, J., Pollak, M., Hartwig, J., and Sever, S. (2010). Direct dynamin-actin interactions regulate the actin cytoskeleton. EMBO J. *29*, 3593–3606.

Harris, J.J., Jolivet, R., and Attwell, D. (2012). Synaptic energy use and supply. Neuron *75*, 762–777.

Hartfuss, E., Galli, R., Heins, N., and Götz, M. (2001). Characterization of CNS precursor subtypes and radial glia. Dev. Biol. *229*, 15–30.

Hartig, F., and Lohse, L. (2020). DHARMa: Residual Diagnostics for Hierarchical (Multi-Level/Mixed) Regression Models. R package version 0.3.2.0. https://cran.r-project.org/web/packages/DHARMa/index.html.

Heinrich, C., Blum, R., Gascón, S., Masserdotti, G., Tripathi, P., Sánchez, R., Tiedt, S., Schroeder, T., Götz, M., and Berninger, B. (2010). Directing astroglia from the cerebral cortex into subtype specific functional neurons. PLoS Biol. *8*, e1000373.

Heinrich, C., Gascón, S., Masserdotti, G., Lepier, A., Sanchez, R., Simon-Ebert, T., Schroeder, T., Götz, M., and Berninger, B. (2011). Generation of subtype-specific neurons from postnatal astroglia of the mouse cerebral cortex. Nat. Protoc. *6*, 214–228.

Heins, N., Malatesta, P., Cecconi, F., Nakafuku, M., Tucker, K.L., Hack, M.A., Chapouton, P., Barde, Y.A., and Götz, M. (2002). Glial cells generate neurons: the role of the transcription factor Pax6. Nat. Neurosci. *5*, 308–315.

Herrero-Mendez, A., Almeida, A., Fernández, E., Maestre, C., Moncada, S., and Bolaños, J.P. (2009). The bioenergetic and antioxidant status of neurons is controlled by continuous degradation of a key glycolytic enzyme by APC/C-Cdh1. Nat. Cell Biol. *11*, 747–752.

Hormanseder, E., Simeone, A., Allen, G.E., Bradshaw, C.R., Figlmuller, M., Gurdon, J., and Jullien, J. (2017). H3K4 Methylation-Dependent Memory of

Somatic Cell Identity Inhibits Reprogramming and Development of Nuclear Transfer Embryos. Cell Stem Cell *21*, 135–143.e6.

Jernberg, J.N., Bowman, C.E., Wolfgang, M.J., and Scafidi, S. (2017). Developmental regulation and localization of carnitine palmitoyltransferases (CPTs) in rat brain. J. Neurochem. *142*, 407–419.

Kaur, S.J., McKeown, S.R., and Rashid, S. (2016). Mutant SOD1 mediated pathogenesis of Amyotrophic Lateral Sclerosis. Gene *577*, 109–118.

Khacho, M., Clark, A., Svoboda, D.S., Azzi, J., MacLaurin, J.G., Meghaizel, C., Sesaki, H., Lagace, D.C., Germain, M., Harper, M.E., et al. (2016). Mitochondrial Dynamics Impacts Stem Cell Identity and Fate Decisions by Regulating a Nuclear Transcriptional Program. Cell Stem Cell *19*, 232–247.

Knobloch, M., Pilz, G.A., Ghesquière, B., Kovacs, W.J., Wegleiter, T., Moore, D.L., Hruzova, M., Zamboni, N., Carmeliet, P., and Jessberger, S. (2017). A Fatty Acid Oxidation-Dependent Metabolic Shift Regulates Adult Neural Stem Cell Activity. Cell Rep. *20*, 2144–2155.

Konermann, S., Brigham, M.D., Trevino, A.E., Joung, J., Abudayyeh, O.O., Barcena, C., Hsu, P.D., Habib, N., Gootenberg, J.S., Nishimasu, H., et al. (2015). Genome-scale transcriptional activation by an engineered CRISPR-Cas9 complex. Nature *517*, 583–588.

Korotkevich, G., Sukhov, V., and Sergushichev, A. (2019). Fast gene set enrichment analysis. bioRxiv. https://doi.org/10.1101/060012.

Lin, R., Tao, R., Gao, X., Li, T., Zhou, X., Guan, K.L., Xiong, Y., and Lei, Q.Y. (2013). Acetylation stabilizes ATP-citrate lyase to promote lipid biosynthesis and tumor growth. Mol. Cell *51*, 506–518.

Liu, J., Su, G., Gao, J., Tian, Y., Liu, X., and Zhang, Z. (2020). Effects of Peroxiredoxin 2 in Neurological Disorders: A Review of its Molecular Mechanisms. Neurochem. Res. *45*, 720–730.

Llorens-Bobadilla, E., Zhao, S., Baser, A., Saiz-Castro, G., Zwadlo, K., and Martin-Villalba, A. (2015). Single-Cell Transcriptomics Reveals a Population of Dormant Neural Stem Cells that Become Activated upon Brain Injury. Cell Stem Cell *17*, 329–340.

Lu, W., Karuppagounder, S.S., Springer, D.A., Allen, M.D., Zheng, L., Chao, B., Zhang, Y., Dawson, V.L., Dawson, T.M., and Lenardo, M. (2014). Genetic deficiency of the mitochondrial protein PGAM5 causes a Parkinson's-like movement disorder. Nat. Commun. *5*, 4930.

Lu, W., Sun, J., Yoon, J.S., Zhang, Y., Zheng, L., Murphy, E., Mattson, M.P., and Lenardo, M.J. (2016). Mitochondrial Protein PGAM5 Regulates Mitophagic Protection against Cell Necroptosis. PLoS ONE *11*, e0147792.

Ma, K., Zhang, Z., Chang, R., Cheng, H., Mu, C., Zhao, T., Chen, L., Zhang, C., Luo, Q., Lin, J., et al. (2020). Dynamic PGAM5 multimers dephosphorylate BCL-xL or FUNDC1 to regulate mitochondrial and cellular fate. Cell Death Differ. *27*, 1036–1051.

Márquez, J., Tosina, M., de la Rosa, V., Segura, J.A., Alonso, F.J., Matés, J.M., and Campos-Sandoval, J.A. (2009). New insights into brain glutaminases: beyond their role on glutamatergic transmission. Neurochem. Int. *55*, 64–70.

Masserdotti, G., Gillotin, S., Sutor, B., Drechsel, D., Irmler, M., Jørgensen, H.F., Sass, S., Theis, F.J., Beckers, J., Berninger, B., et al. (2015). Transcriptional Mechanisms of Proneural Factors and REST in Regulating Neuronal Reprogramming of Astrocytes. Cell Stem Cell *17*, 74–88.

Misgeld, T., and Schwarz, T.L. (2017). Mitostasis in Neurons: Maintaining Mitochondria in an Extended Cellular Architecture. Neuron *96*, 651–666.

Miyake, S., Yamashita, T., Taniguchi, M., Tamatani, M., Sato, K., and Tohyama, M. (2002). Identification and characterization of a novel mitochondrial tricarboxylate carrier. Biochem. Biophys. Res. Commun. *295*, 463–468.

Molinari, F., Raas-Rothschild, A., Rio, M., Fiermonte, G., Encha-Razavi, F., Palmieri, L., Palmieri, F., Ben-Neriah, Z., Kadhom, N., Vekemans, M., et al. (2005). Impaired mitochondrial glutamate transport in autosomal recessive neonatal myoclonic epilepsy. Am. J. Hum. Genet. *76*, 334–339.

Molinari, F., Kaminska, A., Fiermonte, G., Boddaert, N., Raas-Rothschild, A., Plouin, P., Palmieri, L., Brunelle, F., Palmieri, F., Dulac, O., et al. (2009). Mutations in the mitochondrial glutamate carrier SLC25A22 in neonatal epileptic encephalopathy with suppression bursts. Clin. Genet. *76*, 188–194.

Mori, M., Gotoh, S., Taketani, S., Hiai, H., and Higuchi, K. (2013). Hereditary cataract of the Nakano mouse: Involvement of a hypomorphic mutation in the coproporphyrinogen oxidase gene. Exp. Eye Res. *112*, 45–50.

Motori, E., Puyal, J., Toni, N., Ghanem, A., Angeloni, C., Malaguti, M., Cantelli-Forti, G., Berninger, B., Conzelmann, K.K., Götz, M., et al. (2013). Inflammation-induced alteration of astrocyte mitochondrial dynamics requires autophagy for mitochondrial network maintenance. Cell Metab. *18*, 844–859.

O'Connor, R.S., Guo, L., Ghassemi, S., Snyder, N.W., Worth, A.J., Weng, L., Kam, Y., Philipson, B., Trefely, S., Nunez-Cruz, S., et al. (2018). The CPT1a inhibitor, etomoxir induces severe oxidative stress at commonly used concentrations. Sci. Rep. *8*, 6289.

Pagliarini, D.J., Calvo, S.E., Chang, B., Sheth, S.A., Vafai, S.B., Ong, S.E., Walford, G.A., Sugiana, C., Boneh, A., Chen, W.K., et al. (2008). A mitochondrial protein compendium elucidates complex I disease biology. Cell *134*, 112–123.

Poduri, A., Heinzen, E.L., Chitsazzadeh, V., Lasorsa, F.M., Elhosary, P.C., LaCoursiere, C.M., Martin, E., Yuskaitis, C.J., Hill, R.S., Atabay, K.D., et al. (2013). SLC25A22 is a novel gene for migrating partial seizures in infancy. Ann. Neurol. *74*, 873–882.

Rosen, D.R. (1993). Mutations in Cu/Zn superoxide dismutase gene are associated with familial amyotrophic lateral sclerosis. Nature *364*, 362.

Schaffer, A.E., Pinkard, O., and Coller, J.M. (2019). tRNA Metabolism and Neurodevelopmental Disorders. Annu. Rev. Genomics Hum. Genet. *20*, 359–387.

Schmitt, S., Saathoff, F., Meissner, L., Schropp, E.M., Lichtmannegger, J., Schulz, S., Eberhagen, C., Borchard, S., Aichler, M., Adamski, J., et al. (2013). A semi-automated method for isolating functionally intact mitochondria from cultured cells and tissue biopsies. Anal. Biochem. *443*, 66–74.

Spinelli, J.B., and Haigis, M.C. (2018). The multifaceted contributions of mitochondria to cellular metabolism. Nat. Cell Biol. *20*, 745–754.

Tien, A.C., Tsai, H.H., Molofsky, A.V., McMahon, M., Foo, L.C., Kaul, A., Dougherty, J.D., Heintz, N., Gutmann, D.H., Barres, B.A., and Rowitch, D.H. (2012). Regulated temporal-spatial astrocyte precursor cell proliferation involves BRAF signalling in mammalian spinal cord. Development *139*, 2477–2487.

van Deijk, A.F., Camargo, N., Timmerman, J., Heistek, T., Brouwers, J.F., Mogavero, F., Mansvelder, H.D., Smit, A.B., and Verheijen, M.H. (2017). Astrocyte lipid metabolism is critical for synapse development and function in vivo. Glia *65*, 670–682.

Velletri, T., Romeo, F., Tucci, P., Peschiaroli, A., Annicchiarico-Petruzzelli, M., Niklison-Chirou, M.V., Amelio, I., Knight, R.A., Mak, T.W., Melino, G., and Agostini, M. (2013). GLS2 is transcriptionally regulated by p73 and contributes to neuronal differentiation. Cell Cycle *12*, 3564–3573.

Vignoles, R., Lentini, C., d'Orange, M., and Heinrich, C. (2019). Direct Lineage Reprogramming for Brain Repair: Breakthroughs and Challenges. Trends Mol. Med. *25*, 897–914.

Walcher, T., Xie, Q., Sun, J., Irmler, M., Beckers, J., Öztürk, T., Niessing, D., Stoykova, A., Cvekl, A., Ninkovic, J., and Götz, M. (2013). Functional dissection of the paired domain of Pax6 reveals molecular mechanisms of coordinating neurogenesis and proliferation. Development *140*, 1123–1136.

Wiśniewski, J.R., Zougman, A., Nagaraj, N., and Mann, M. (2009). Universal sample preparation method for proteome analysis. Nat. Methods *6*, 359–362.

Wu, J., Ocampo, A., and Belmonte, J.C.I. (2016). Cellular Metabolism and Induced Pluripotency. Cell *166*, 1371–1385.

Zhang, X., Smits, A.H., van Tilburg, G.B., Ovaa, H., Huber, W., and Vermeulen, M. (2018). Proteome-wide identification of ubiquitin interactions using UbIA-MS. Nat. Protoc. *13*, 530–550.

Zischka, H., Larochette, N., Hoffmann, F., Hamöller, D., Jägemann, N., Lichtmannegger, J., Jennen, L., Müller-Höcker, J., Roggel, F., Göttlicher, M., et al. (2008). Electrophoretic analysis of the mitochondrial outer membrane rupture induced by permeability transition. Anal. Chem. *80*, 5051–5058.

STAR★METHODS

KEY RESOURCES TABLE

REAGENT or RESOURCE	SOURCE	IDENTIFIER
Antibodies		
Rabbit anti-CS	Novus Biologicals	NBP2-13878
Rabbit anti-VDAC	Cell Signaling	Cat# 4866; RRID: AB_2272627
Goat anti-ANT	Santa Cruz	Cat# sc.9299; RRID: AB_671086
Total Oxphos Rodent Ab cocktail	Abcam	Cat# ab110413; RRID: AB_2629281
Mouse anti-β-III-Tubulin	Sigma-Aldrich	Cat# T8660; RRID: AB_477590
Mouse anti-GFAP	Dako	Cat# Z0334; RRID: AB_100013482
Rabbit anti-GFAP	Sigma-Aldrich	Cat# G3893; RRID: AB_477010
Rat anti-RFP	Chromotek	Cat# 5F8; RRID: AB_2336064
Rabbit anti-RFP	Rockland	Cat# 600-401-379; RRID: AB_2209751
Chicken anti-GFP	Aves Labs	Cat# GFP-1020; RRID: AB_10000240
Rabbit anti-CPOX	Abcam	Cat# Ab169766
Rabbit anti-Prdx2	Abcam	Cat# Ab109367; RRID: AB_10862524
Rabbit anti-Gls	Proteintech	Cat# 20170-1-AP; RRID: AB_10665373
Rabbit anti-Sfxn5	Abcam	Cat# Ab172971
Anti-Aldh1l1	Merck Millipore	Cat# MABN495; RRID: AB_2687399
Anti-Tomm20	Abnova	CAt# H00009804-M01; RRID: AB_1507602
Anti-Mouse-HRP linked	Invitrogen	Cat#626520; RRID: AB_2533947
Anti-Mouse, HRP linked	Cell Signaling	Cat# 7076; RRID: AB_330924
Anti-Rabbit, HRP linked	Cell Signaling	Cat# 7074; RRID: AB_2099233
Anti-Rabbit, HRP, linked	GE Healthcare	Cat#NA934; RRID: AB_2722659
Anti-Goat, HRP linked	Santa Cruz	Cat# sc-2020; RRID: AB_631728
Anti-Mouse Alexa Fluor 488	Molecular Probes	Cat# A-21202; RRID: AB_141607
Anti-Chicken Alexa Fluor 488	Thermo Fisher	Cat# A-11039; RRID: AB_2534096
Anti-Rat Cy3	Dianova	Cat# 112-165-167; RRID: AB_2338251
Anti-Mouse IgG2b 633	Innovative Research	Cat# A21146; RRID: AB_1500899
Anti-Mouse IgG1 647	Molecular Probes	Cat# A21240; RRID: AB_141658
Anti-Rabbit Alexa Fluor 488	Molecular Probes	Cat# A21206; RRID: AB_141708
Anti-Mouse IgG1 Biotin	Southernbiotech	Cat# 1070-08; RRID: AB_2794413
Streptavidin Alex Fluor 405	Thermo Fisher	Cat# S32351
Bacterial and Virus Strains		
RV CAG-Neurog2-ires-DsRedExpress2	Gascón et al., 2016	N/A
RV CAG-Ascl1-ires-DsRed	Gascón et al., 2016	N/A
RV CAG-DsRedExpress2	Gascón et al., 2016	N/A
RV CAG-mitoGFP	This study	N/A
RV CAG-Ascl1-ires-mitoGFP	This study	N/A
RV CAG-Ascl1-ires-mitoRFP	This study	N/A
Chemicals, Peptides, and Recombinant Proteins		
EGF	GIBCO	Cat# PHG0311
bFGF	GIBCO	Cat# 13256029
Poly-D-Lysine	Sigma-Aldrich	Cat# P0899
B27	GIBCO	Cat# 17504044
HBSS medium	Thermo Fisher	Cat# 24020117
HEPES	Thermo Fisher	Cat# 15630080
DMEM/F12	Thermo Fisher	Cat# 10565018

(*Continued on next page*)

Continued

REAGENT or RESOURCE	SOURCE	IDENTIFIER
trypsin/EDTA 0,25%	Thermo Fisher	Cat# 25200056
Neurobasal Medium	GIBCO	Cat# 21103149
Glucose	GIBCO	Cat# A2494001
GluataMAX	GIBCO	Cat# 35050061
OptiMEM – GlutaMAX	Thermo Fisher	Cat# 51985-026
EGTA	Sigma-Aldrich	Cat# E3889
Lipofectamine 2000	Thermo Fisher	Cat# 11668019
Rhodamine 123	Thermo Fisher	Cat# R302
Oligomycin A	Sigma-Aldrich	Cat# 73351
FCCP	Sigma-Aldrich	Cat# C2920
Rotenone	Sigma-Aldrich	Cat# R8875
Antimycin A	Sigma-Aldrich	Cat# A8674
2-Deoxy-D-glucose	Sigma-Aldrich	Cat# D8375
Triton X-100	Sigma-Aldrich	Cat# T9284
Etomoxir	Sigma-Aldrich	Cat# E1905
Bovine Serum Albumine (BSA)	Sigma-Aldrich	Cat# A9418
Critical Commercial Assays		
Arcturus PicoPure RNA Isolation Kit	Thermo Fisher	Cat# 12204-01
Bradford Protein Assay Kit	BioRad	Cat# 5000201
First Strand cDNA Synthesis Kit	Thermo Fisher	Cat# K1621
PowerUp SYBR Green Master Mix	Thermo Fisher	Cat# A25742
Agencourt AMPure XP	Beckman Coulter	Cat# 10136224
RC DC Protein assay	BioRad	N/A
Deposited Data		
mitoProteomic data, identifier: PXD014886	This study	https://www.ebi.ac.uk/pride
Experimental Models: Organisms/Strains		
C57BL/6	LMU animal Facility	N/A
Aldh1l1-Cre	LMU animal Facility	N/A
Rosa26-LoxP-Stop-LoxP-dCAM	HMGU	N/A
Oligonucleotides		
See Methods S1	This study	N/A
Recombinant DNA		
STAgR_Neo	Addgene	RRID:Addgene_102992
STAGR_gRNAScaffold_hU6	Addgene	RRID:Addgene_102843
STAGR_gRNAScaffold_hH1	Addgene	RRID:Addgene_102841
STAGR_gRNAScaffold_h7SK	Addgene	Addgene_102841
STAGR_gRNAScaffold_mU6	Addgene	RRID:Addgene_102844
pCDNA-miniCMV-GFP	This study	N/A
STAgR_cntrl	This study	N/A
STAgR_Acot7	This study	N/A
STAgR_Arg2	This study	N/A
STAgR_Gls	This study	N/A
STAgR_Mgst3	This study	N/A
STAgR_Pgam5	This study	N/A
STAgR_Sod1	This study	N/A
STAgR_Slc25a22	This study	N/A
STAgR_Dnm3	This study	N/A
STAgR_Mgst1	This study	N/A
STAgR_Prdx6	This study	N/A

(*Continued on next page*)

Continued

REAGENT or RESOURCE	SOURCE	IDENTIFIER
STAgR_Arg2-Gls (A-G)	This study	N/A
STAgR_Prdx2-Sod1 (P-S)	This study	N/A
STAgR_Arg2-Dnm3 (A-D)	This study	N/A
Software and Algorithms		
ZEN software	Zeiss	https://www.zeiss.com/microscopy/en_us/products/microscope-software/zen.html RRID:SCR_013672
ImageJ	ImageJ	https://imagej.net/Downloads RRID: SCR_003070
Morphometric analysis	SNT	Ferreira et al., 2014
Sholl Analysis	ImageJ	N/A
Co-localizatioin	Coloc2	https://imagej.net/Coloc_2
Proteome discoverer 2.2 software	Thermo Fisher	https://www.thermofisher.com/order/catalog/product/IQLAAEGABSFAKJMAUH RRID:SCR_014477
SwissProt Database Mouse	NCBI Protein	https://www.ncbi.nlm.nih.gov/protein RRID:SCR_003257
mitoCARTA 2.0 database	Calvo et al., 2016)	N/A
Perseus Software	Perseus	http://maxquant.net/perseus/ RRID:SCR_015753
GraphPad Prism 7.0	GraphPad Software	https://www.graphpad.com:443/ RRID:SCR_002798
Adobe Illustrator	Adobe Illustrator	https://www.adobe.com/de/products/catalog.html RRID:SCR_010279
Zeiss AxioVision 4.7 software	Zeiss	http://www.zeiss.com/microscopy/us/products/microscope-software/zen-core.html?vaURL=www.zeiss.com/microscopy/us/products/microscope-software/axiovision.html
Microsoft Excel	Microsoft Excel	https://www.microsoft.com/en-gb/ RRID:SCR_016137
Seahorse Wave	Agilent Technologies	https://www.agilent.com/en-us/products/cell-analysis-(seahorse)/software-download-for-wave-desktop RRID:SCR_014526
RStudio		https://rstudio.com
	DHARMa	https://cran.r-project.org/web/packages/DHARMa/vignettes/DHARMa.html
	DEP	https://www.bioconductor.org/packages/release/bioc/html/DEP.html
	ggplot2	https://ggplot2.tidyverse.org
	Pheatmap	https://www.bioconductor.org/packages/release/bioc/html/heatmaps.html
	fgsea	https://bioconductor.org/packages/release/bioc/html/fgsea.html
	TopGo	https://bioconductor.org/packages/release/bioc/html/topGO.html
Other		
Aqua Poly/Mount	Polysciences	Cat# 18606-20

RESOURCE AVAILABILITY

Lead Contact

Further information and requests for resources and reagents should be directed to and will be fulfilled by the Lead Contact, Prof. Magdalena Götz (magdalena.goetz@helmholtz-muenchen.de).

Materials Availability

- Plasmids generated in this study are available upon request.
- gRNA sequences used to activate gene-specific loci are listed in Methods S1.
- Aldh1-Cre transgenic mice are available at Jackson Lab (stock n.023748).
- There are restrictions to the availability of dCAM mice due to MTA request.

Data and Code Availability

- Mass spectrometry proteomics data have been deposited to the ProteomeXchange Consortium via the PRIDE, partner repository, with dataset identifier PXD014886.

EXPERIMENTAL MODEL AND SBJECT DETAILS

Wild-type mice (Primary Cell culture, Proteomics, IHC)

All experimental procedures in this study, done at the LMU München, were performed in accordance with German and European Union guidelines and were approved by the government of Upper Bavaria. For most of the experiments, primary cultures of astrocytes were obtained from brains of C57BL/6J mice of 5-7 days of age; no specific gender was considered. Primary cultures of cortical neurons were obtained from brains of C57BL/6J embryos at 14.5 days post conception (14.5 dpc or E14.5). Mice were fed *ad libitum* and housed with 12/12 h light and dark cycle and kept under specific-pathogen-free (SPF) conditions.

Aldh1-Cre and Cre-inducible dCas9-VPR mice

The activation of specific mitochondria-coding genes was performed in primary cultures of astrocytes obtained from Aldh1l1-Cre (Tien et al., 2012) crossed with dCAM mice (Rosa26-loxP-Stop-LoxP-dCas9VPR-SAM mice (J.G.-S., unpublished data). Both strains were used as heterozygotes. The background strain of the mice was C57BL/6.

Primary cultures of cortical astrocytes

Astrocytes were isolated and cultured as previously described, with small changes (Heins et al., 2002). After removal of the meninges, gray matter tissue from cerebral cortex of C57BL/6J mice at postnatal day 5-7 (P5–P7) was dissected and dissociated mechanically. Subsequently, cells were centrifuged for 5 min at 1,300 rpm, re-suspended, and plated in a T25 flask in medium consisting of DMEM/F12 (1:1), 10% fetal bovine serum (FBS), penicillin /streptomycin, and 1x B27 serum-free-supplement, 10 ng/ml epidermal growth factor (EGF), and 10 ng/ml basic fibroblast growth factor (bFGF) (astro-medium). Cells were passaged at 80%–90% confluency after 7-10 days using trypsin/EDTA and plated on poly-D-lysine coated glass coverslips at a density of 50,000-60,000 cells per coverslip (in 24-well plates) in fresh astro-medium. The vast majority of the cells (> 90%) in these cultures were positive for glial fibrillary acidic protein (Gfap) as previously described. Primary cultures of astrocytes were maintained in an incubator for 6-8 days at 37°C and 5% CO_2.

Cells undergoing direct neuronal conversion

One day after transduction or transfection, astro-medium was replaced with fresh medium consisting of DMEM/F12 (1:1), penicillin/streptomycin, supplemented with 1x B27 and Glutamax, but not FBS, EGF and FGF (differentiation medium). Small molecules were added once, at the time of medium replacement (24h after transduction or transfection). Cultures were maintained in an incubator for 6-8 days at 37°C and 9% CO_2.

Primary cultures of cortical neurons

Cerebral cortices were dissected from embryonic day (E) 14 mice as described before (Hartfuss et al., 2001; Walcher et al., 2013). Cortices were isolated, meninges removed and samples mechanically dissociated in 1x HBSS medium containing 10mM HEPES, on ice. Subsequently, cells were digested for 15 min in trypsin-EDTA (0.05%) and centrifuged for 5 min at 1,000 rpm. The pellet was resuspended in medium containing 10% FBS to stop trypsin, then centrifuged again and resuspended in 1x Neurobasal Medium, supplemented with 1x Glutamax, penicillin/streptomycin, and 1x B27. Cells were counted and plated at a density of 600,000 cells per well in 6-well plates, pre-coated with poly-D-lysine. After one week in culture the cells had mostly differentiated into neurons, with a high purity and little contamination by other cell types.

METHOD DETAILS

Transfection and Transduction

For transfection, DNA-liposome complexes were prepared in OptiMem medium using the retroviral plasmids described below and Lipofectamine 2000. Astrocytic cultures, plated the day before in 24-well plates at a density of 60,000-80,000 cells per well, were transfected with DNA-liposome complexes composed of 0.6 μg total DNA, mixed with 0,75μl of Lipofectamine2000 per well, in 400μl of OptiMem medium for 4 hours. Then, transfection medium was replaced by a solution composed to 1:1 ratio of fresh astro-medium and astro-medium collected from the same cells before the transfection (and filtered). One day later, the medium was replaced with differentiation medium and cells maintained in culture until 6-7 days post-transfection in 9% CO_2 incubator. For FACSorting, RNA extraction and RT-PCR, astrocytes were plated in 6-well plates pre-coated with PDL at a concentration of 350,000 cells per well. The following day, cells were transfected with DNA-liposome complexes containing 1μg total DNA and 1,25μl Lipofectamine 2000 per 1ml of OptiMem medium for 4 hours and cultured in astro-medium for 48hours before sorting. For STAgR experiments, primary cultures of astrocytes, obtained from double positive Aldh1l1-Cre dCAM mice (Rosa26-loxP-Stop-LoxP-dCas9VPR-SAM mice (Giehrl-Schwab J. et al., in revision), were transfected with plasmids encoding the indicated STAgR and Ascl1 with a molar ratio 1:1. For transduction, astrocytes were infected with 1μl of virus per well one day after plating. The viruses used are listed in the key resource table and were produced as previously described (Gascón et al., 2016).

Fluorescence-activated Cell Sorting

WT astrocytes were transfected with gRNAs-GFP and dCas9-VPR-DsRed plasmids. Cells were collected 48 hours after transfection and sorted for RFP^+/GFP^+, using the FACSAria III (BD Bioscience) system at high purity mode and a flow rate lower than 600 cells per second. Alternatively, astrocytes obtained from Aldh1l1-Cre x dCAM transgenic mice were transfected only with gRNA-expressing plasmids and subjected to FACS analysis at 48 hours, collecting GFP+ cells. Cells were washed twice with 1x PBS, treated with trypsin (0,05% in EDTA) for 5%, then astro-medium was added. Cells were harvested by centrifugation (1,000 rpm, 5min, 4°C), washed twice with 1x PBS and, then, resuspended in 400μl of DMEM/F12 (1:1), phenol-red-free. Single cell suspension was filtrated using a 70-μm cell strainer. Cells were sorted using the FACS Aria III (BD). Gates were set by using un-transfected cells, as well cells expressing GFP or DsRed as positive control. 15,000 cells were sorted directly in extraction buffer (Picopure RNA isolation kit) to enhance RNA quality and efficiency, for subsequent extraction and qRT-PCR.

Mitochondria isolation

Mitochondria isolation from cultured astrocytes and neurons was performed as previously described (Schmitt et al., 2013) using the pump-controlled cell (PCC) rupture method; a cell homogenizer (Isobiotec, Germany) combined with 1 mL Luer Lock Gas-Tight Syringes (4.608 mm i.d., SGE Supelco, USA) and a high-precision pump (Pump 11, Harvard Apparatus, USA). The homogenizer was pre-cooled on ice to ensure cooling of the samples during the isolation, the tungsten carbide ball (6um diameter) was inserted and the homogenizer was equilibrated with isolation buffer (300 mM sucrose, 5 mM TES, and 200 μM ethyleneglycoltetraacetic acid [EGTA], pH 7.2). The sample of dissociated astrocytes or neurons was added to 1 mL of isolation buffer and passed three (neurons) to six (astrocytes) times through the system at a constant rate (700 μl/min). To recover the homogenate, the system was rinsed once with 1 mL of isolation buffer. The sample preparation and the tunable parameters of the PCC, such as the clearance and the number of strokes, were optimized for each sample. Yield and functionality (mitochondrial transmembrane potential, $\Delta\psi_m$) of the isolated mitochondria were used to assess the optimal parameters. Around 1 million astrocytes and neurons respectively were used to obtain a sufficient amount of mitochondria for further processing. The pooled homogenate was cleared from cell debris and nuclei by centrifugation (800 × *g*, 5 min at 4°C), and mitochondria were pelleted at 9000 × *g* (10 min at 4°C). After the isolation, syringes were rinsed 3-4 times with double distilled water (ddH_2O). The tungsten carbide ball and the cell homogenizer were cleaned with isopropanol followed by ddH_2O to allow processing of the next sample without contamination.

Characterization of isolated mitochondria

The functional analysis of isolated mitochondria was performed by measuring Rhodamine 123 (Rh123) fluorescence quenching in order to determine $\Delta\psi_m$, as well as measuring the absorbance change at 540nm (Synergy 2, BioTek, USA) to determine mitochondrial swelling, as described previously (Schmitt et al., 2013). Protein concentrations were determined by the Bradford assay. For immunoblotting analysis, 10 μg of protein was subjected to sodium dodecyl sulfate-polyacrylamide gel electrophoresis (SDS-PAGE), and separated proteins were transferred onto PVDF membrane. Equal protein loading and proper transfer were controlled by Ponceau red staining. The primary and secondary antibodies used for Western Blot analysis are listed in the Key Resource table.

Electron microscopy analysis of the isolated mitochondria was done as described previously (Zischka et al., 2008). ZE-FFE-separated mitochondrial fractions were immediately pelleted, fixed in 2.5% glutaraldehyde, post-fixed with 1% osmium tetroxide, dehydrated with ethanol and embedded in Epon. Ultrathin sections were negatively stained with uranyl acetate and lead citrate and then analyzed on a Zeiss EM 10 CR electron microscope.

Seahorse experiments

Primary cortical astrocytes or neurons were plated onto XF24 V3 PET cell culture microplates from Seahorse biosciences, pre-coated with PDL, and analyzed the day after plating. Cells were seeded at 20,000, 30,000, 50,000 for neurons; and 15,000, 25,000 or 40,000 for astrocytes. The final cell number was assessed by counting $DAPI^+$ nuclei and measuring DNA content to normalize the data to μg DNA or 1000 cells. Before measuring cellular respiration, cells were washed twice with assay medium (XF DMEM + 25 mM glucose) and then incubated in 750 μL of assay medium for 10 min in an air incubator without CO_2 at 37°C. The XF24 plate was then transferred to the XF24 Extracellular Fluxanalyzer (Seahorse Bioscience). Basal respiration was determined with 4-5 assay cycles (2 min. mix, 2 min. measuring), and all parameters were obtained after the respective drug application. Basal OCR and PPR were measured prior to oligomycin treatment. For the measurement of different mitochondrial respiration states, oligomycin A (Oligo, 5 μg/ml) was used to inhibit the ATP synthase, followed by Carbonyl cyanide-*4*-(trifluoromethoxy)phenylhydrazone (FCCP, 1 μM) to induce maximal substrate oxidation capacity, and a cocktail containing rotenone (Rot, 5 μM) and antimycin A (Ant, 2 μM) to inhibit ETC activity and determine non-mitochondrial oxygen uptake. Finally, 2-deoxyglucose (2-DG, 100mM) was added to block glycolysis. Extracellular acidification rate (ECAR) was converted to proton production rate (PPR) based on machine algorithms and the buffer capacity of the medium. The OCR/PPR ratio was calculated over the averaged basal values. Each value is calculated averaging 3-5 time points from 3 technical replicates.

Proteome analysis

Isolated mitochondria (10 μg) were used per biological replicate. SDS was added to a final concentration of 2% for efficient solubilization, prior to tryptic protein digest using a modified FASP protocol (Wiśniewski et al., 2009). Proteomic measurements were performed on a Q-Exactive HF mass spectrometer (Thermo Scientific) online coupled to an Ultimate 3000 nano-RSLC (Dionex). Peptides

were separated on a C18 nanoEase MZ HSS T3 column (100Å, 1.8 μm, 75 μm x 250 mm; Waters) in a 95 min non-linear acetonitrile gradient. Precursor (scan range 300 – 1500 m/z) and TOP10 fragment spectra of charges 2-7 were acquired in the orbitrap mass detector of the mass spectrometer, at resolutions of 60,000 and 15,000 respectively with a maximum injection time of 50 ms and a dynamic exclusion of 30 s for each one. The individual raw-files were loaded to the Proteome discoverer 2.2 software (Thermo scientific) allowing for peptide identification and label-free quantification using the Minora node. Searches were performed using Sequest HT as a search engine in the Swissprot mouse database with the following search settings: 10 ppm precursor tolerance, 0.02 Da fragment tolerance, two missed cleavages allowed, carbamidomethyl on cysteine as fixed modification, deamidation of glutamine and asparagine allowed as variable modification, as well as oxidation of methionine and Met-loss combined with acetylation at the N terminus of the protein. Proteins were quantified by summing up the abundances of allocated unique and razor peptides; resulting protein abundances are given in Table S1. Mitochondrial proteins were classified using the mitoCARTA 2.0 database (Calvo et al., 2016). Data were analyzed in RStudio (version 3.5.3), using the package DEP (Zhang et al., 2018). First, we filtered for proteins identified in all replicates of at least one condition; then, data were normalized using variance stabilizing transformation (vsn). Differential enrichment analysis was performed based on linear model. Identified proteins were considered as enriched in neurons if the log2(fold-change value) was > 1 and enriched in astrocytes if the log2(fold-change value) was < −1 and pvalue < 0.05 (according to DEP output). Differentially enriched proteins (DEP) data are provided in Table S1. *T*-Distributed Stochastic Neighbor Embedding (*t*-SNE) was computed from data normalized in DEP package in RStudio, as well as the heatmap of all considered proteins and the distance matrix including hierarchical clustering. Gene Ontology analysis was performed in RStudio using the package "TopGO," using exact Fisher test. Proteins were considered differentially enriched if log2(fold-change) > |1| and pval < 0.05. Complete list of GO term is provided in Table S2. For Gene Set Enrichment Analysis (GSEA) the package "fgsea" in Rstudio was employed (Korotkevich et al., 2019). Complete list of GSEA term is provided in Table S2*E*.

Western Blot Analysis

Primary cultures of astrocytes or neurons were collected and lysed in RIPA buffer. Protein concentration was evaluated with RC DC Protein assay (Bio-Rad Laboratories); 60μg of lysate was loaded in sodium dodecyl sulfate-polyacrylamide gel electrophoresis (SDS-PAGE) and transferred onto a polyvinylidene fluoride (PVDF) membrane. Depending on the size of the protein analyzed, different gel concentration was used. The primary and secondary antibodies used for Western Blot analysis are listed in Key Resources Table.

Immunocytochemistry

Cells were fixed in 4% paraformaldehyde (PFA) in PBS1X for 10 min. at room temperature, washed in PBS1X twice for 5 minutes, and stored up to a month at 4°C before staining. For Prdx2 staining, cells were fixed in ice-cold Methanol 20% for 10 minutes, washed twice in PBS1X for 10 minutes, and subsequently stored and treated as other samples. Specimen were incubated in primary antibodies (for concentration see Key Resources Table) in PBS1X containing 3% Bovine Serum Albumin (BSA) and 0.5% Triton X-100 for 2 hours at room temperature or overnight at 4°C. After washing twice for 5 minutes with PBS, cells were incubated with the appropriate species- or subclass-specific secondary antibodies, with or without DAPI to label nuclei (blue), diluted 1:10000, for 1 hour in the dark at room temperature. Optionally, after incubating with primary antibodies and washing with PBS, biotin-labeled secondary antibodies were used at a dilution of 1:200 for 1 hour, followed by streptavidin-coupled fluorophores (1:500) for another hour. Coverslips were then mounted with Aqua Poly/Mount (Polysciences, Warrington, PA). Samples were imaged at the LSM710 laser-scanning confocal or Axio Observer Z1 epifluorescence microscope (Carl Zeiss). Digital images were acquired using the ZEN software (Carl Zeiss) at 80X, 40X or 25x.

RNA extraction, retro-transcription and Real Time Quantitative PCR (qRT-PCR)

RNA was extracted using Arcturus PicoPure RNA Isolation Kit (Thermo Fisher Scientific) according to the manufacturer's instructions, including removal of genomic DNA. 100ng RNA was reverse transcribed using the ThermoFisher cDNA first strand kit. Each cDNA sample was diluted 1:5. qPCR reactions were performed on an Applied Biosystems QuantStudio 6 Flex Real-Time PCR System, or Roche LightCycler 480. Each 10 μL reaction consisted of 5 μL of PowerUp SYBR Green Master Mix (Thermo Fisher), 0.05 μL of forward and reverse primer (100 μM) and 5 μL of DNA appropriately diluted. qRT-PCR primers can be found in Key Resource table. The expression of each gene was analyzed in triplicate. Data were subjected to normalization by using *Gapdh* as housekeeping genes and expressed as mRNA fold change compared to control. Quantification was performed on 3 independent biological samples, each time as technical triplicate. Off targets were selected from the UCSC genome browser, potentially targeting intergenic as well as exon regions. Primers are listed in Methods S1.

STAgR cloning

For generation of STAgR cloning fragments, we followed previously published protocols (Breunig et al., 2018a, 2018b; Gibson, 2011). In particular, we generated individual cloning fragments for Gibson assembly by PCRs on 10 ng of vector templates (STAgR_Neo, STAGR_gRNAScaffold_hU6, STAGR_gRNAScaffold_hH1, STAGR_gRNAScaffold_h7SK and/or STAGR_gRNAScaffold_mU6). The mix contained 10 μl of high fidelity (HF) buffer, 1 μl of 10 mM dNTPs, 0.25 μl of overhang-primers (see key resources), 0.5 μl of HF polymerase, 1.5 μl of dimethyl sulfoxide (DMSO) and enough H_2O to reach a final volume of 50 μl. Reactions were incubated on a thermocycler as follows: 1 cycle of 98°C for 1 min 30 s; 38 cycles of 98°C for 10 s, 59°C (for gRNA scaffold)/ 68°C (for SAM loop) for 10 s, 72°C for 30 s (for inserts) / 1 min 30 s (for vectors); 1 cycle of 72°C for 10 min. 44.5 μl of the PCR reaction were mixed

with 0.5 μl of DpnI enzyme (10 units) and 5 μl of buffer, then incubated for 1 h at 37°C. DNA purification was achieved through incubation with 90 μl of magnetic beads for 2 min at room temperature (RT). Beads were pelleted through a magnet and washed twice with 70% ethanol without complete resuspension. The pellet was then dissolved in 20μl H_2O and separated from the beads. DNA concentration was measured using a spectrophotometer. Gibson Assembly has been performed following a homemade Gibson assembly mix. The 5x isothermal reaction buffer is composed as follows: 1 M Tris (Tris(hydroxymethyl)aminomethane)-HCl (pH 7.5), 300 μl of 1 M MgCl, 60μl of 100 mM dGTP (deoxyguanosine triphosphate), 60 μl of 100 mM dATP (deoxyadenosine triphosphate), 60 μl of 100 mM dTTP (deoxythymidine triphosphate), 60 μl of 100 mM dCTP (deoxycytidine triphosphate), 300 μl of 1 M DTT (dithiothreitol), 1.5 g of PEG-8000 (polyethylene glycol), 300 μl of 100 mM NAD (nicotinamide adenine dinucleotide) and enough H_2O to obtain 6 ml. For the assembly master mix, 320 μl of 5x isothermal reaction buffer was combined with 697 μl of H_2O, 3 μl of 10 U/μl T5 exonuclease, 20 μl of 2 U/μl DNA polymerase and 160 μl of 40 U/μl Taq DNA ligase. 7.5 μl of assembly master mix have been mixed with 2.5 μl of insert and vector. A vector to insert ratio of 1:3 was used. Samples were incubated at 50°C for 60 min and subsequently transformed into *E. Coli*. Resulting plasmids have been sequenced by the Sanger sequencing method with the following primers: StAgR_seq_fwd1 (GAGTTAGGGGCGGGACTATG), StAgR_seq_fwd2 (ACTGGATCCGGTACCAAGG) and StAgR_seq_rev (TTACGGTTCCTGGCCTTTTG). Verified inserts have been cut with KpnI and subcloned into pCDNA-miniCMV-GFP. Primers for gRNA are listed in Methods S1 table.

Live-Imaging Microscopy

Continuous live imaging was performed with a Cell Observer (Zeiss) at a constant temperature of 37°C and at 5% CO_2. Phase-contrast images were acquired every 10 min and fluorescence pictures every 4 hours for 6 days using a 10x phase contrast objective (Zeiss) and an AxioCam HRm camera with a self-written VBA module remote controlling Zeiss AxioVision 4.7 software (TAT, Prof. Dr. Timm Schroeder). Movies were assembled and analyzed using ImageJ (NIH) software, as also described in Gascón et al. (2016). In Figure 4B data are shown as pool of five independent biological replicates; in Figures 4C–4G all cells considered from all biological replicates are shown, indicated by different colors; statistics was performed on the 5 biological replicates using linear regression in Rstudio (see below).

QUANTIFICATION AND STATISTICAL ANALYSIS

When virus was used to induce neuronal conversion (Figure 1; Figure S2; Figure 3; Figure S3; Figure 4), astrocytes were fixed at the days after transduction, as indicated in the figures. Quantification for neuronal cells was based on β-III-tubulin immunoreactivity and morphological parameters, e.g., appearance of processes longer than 3x the cell soma as in Gascón et al. (2016). Astrocytes were quantified based on morphological features and Gfap expression, though Gfap is downregulated following direct conversion. For quantification in Figure 2 and Figure S2, we selected 10 transduced cells per each condition (DsRed, Ascl1-ires-DsRed at day 1 and day 3, and DsRed, Ascl1-ires-DsRed with neuronal morphology or astrocytic morphology at day 5 and 7). ImageJ (v1.52p) was used to define a region of interest (ROI) outlining a selected cell in order to measure the signal intensity for a given protein. To prevent a possible bias due to the different mitochondrial content in astrocytes and neurons, we also evaluated the intensity of Tomm20, a pan-mitochondrial protein. For each ROI, after subtracting the background value, we divided the intensity of the protein of interest by the corresponding Tomm20 expression, and log transformed the value. The colocalization analysis was conducted using the Coloc2 plugin for ImageJ.

For time-lapse experiment quantifications (Figure 4 and Figure S4), cells were tracked in every frame of the movie. $GFP^+/DsRed^+$ cells acquiring neuronal morphology, with processes longer than 3x the cell soma, were quantified among the total $GFP^+/DsRed^+$ cells, as previously published (Gascón et al., 2016). In total, 158 cells were tracked in controls and 177 in Ascl1+Prdx2-Sod1 over n = 5 biological replicates.

Morphological analysis of reprogrammed neuronal cells (Figures 3F–3H) was performed with the ImageJ plugin SNT (simple Neurite tracer) (Ferreira et al., 2014) and different parameters were measured. Sholl analysis, also in ImageJ, was performed on each of the traced neurons: a step size of 10μm was maintained constant, with the first radius defined according to the soma of each cell. We evaluated 3-4 neurons per condition, in 4 biological replicates. Data were analyzed with Microsoft Excel, GraphPad Prism 7.0 software and linear regression using "lm" function (R Stats package) in RStudio. Evaluation of the residuals for fitted linear models was performed with the package "DHARMa" (Hartig and Lohse, 2020) in RStudio.

Statistics on the reprogramming efficiency in Figure S2 and Figure 4 was performed as follows: reprogramming efficiency was log2 transformed, in order to reduce differences in variance across experiments and to fit the data to a normal distribution. Then, linear regression model was used, together with "DHARMa" package to evaluate the residuals. Statistics on Figure 2 and Figure S3 was perfomerd log2-transformed ratio. Statistics on Figure 4 was evaluated using paired t test. The number of biological replicates is indicated in the corresponding Figure legends. Data are plotted as mean ± standard error of the mean (SEM). Significance is based on the p value indicated on the graphs as * $p \leq 0.05$, ** $p \leq 0.01$, ***$p \leq 0.001$.